Thioredoxin-Mediated ROS Homeostasis Explains Natural Variation in Plant Regeneration[1][OPEN]

Hui Zhang,[2] Ting Ting Zhang,[2] Hui Liu,[2] De Ying Shi, Meng Wang, Xiao Min Bie, Xing Guo Li,[3] and Xian Sheng Zhang[3]

State Key Laboratory of Crop Biology, College of Life Sciences, Shandong Agricultural University, Tai'an 271018, China

ORCID IDs: 0000-0002-0518-9266 (H.Z.); 0000-0003-0222-8650 (T.T.Z.); 0000-0002-5693-9397 (H.L.); 0000-0003-4183-555X (D.Y.S); 0000-0002-9730-5550 (M.W.); 0000-0003-0256-0434 (X.M.B.); 0000-0002-1953-4243 (X.G.L.); 0000-0002-3129-5206 (X.S.Z.).

Plant regeneration is fundamental to basic research and agricultural applications. The regeneration capacity of plants varies largely in different genotypes, but the reason for this variation remains elusive. Here, we identified a novel thioredoxin DCC1 in determining the capacity of shoot regeneration among Arabidopsis (*Arabidopsis thaliana*) natural variation. Loss of function of *DCC1* resulted in inhibited shoot regeneration. *DCC1* was expressed mainly in the inner tissues of the callus and encoded a functional thioredoxin that was localized in the mitochondria. DCC1 protein interacted directly with CARBONIC ANHYDRASE2 (CA2), which is an essential subunit of the respiratory chain NADH dehydrogenase complex (Complex I). DCC1 regulated Complex I activity via redox modification of CA2 protein. Mutation of *DCC1* or *CA2* led to reduced Complex I activity and triggered mitochondrial reactive oxygen species (ROS) production. The increased ROS level regulated shoot regeneration by repressing expression of the genes involved in multiple pathways. Furthermore, linkage disequilibrium analysis indicated that DCC1 was a major determinant of the natural variation in shoot regeneration among Arabidopsis ecotypes. Thus, our study uncovers a novel regulatory mechanism by which thioredoxin-dependent redox modification regulates de novo shoot initiation via the modulation of ROS homeostasis and provides new insights into improving the capacity of plant regeneration.

Plant cells have the capacity to regenerate new shoots from highly differentiated tissues or organs under suitable conditions, a process known as shoot regeneration (Birnbaum and Alvarado, 2008; Duclercq et al., 2011). Shoot regeneration normally includes two steps (Ikeuchi et al., 2016). The first step is callus formation, which is regulated by a number of transcription factors, such as WUSCHEL RELATED HOMEOBOX5 (WOX5), WOX11, and WOX12 (Sugimoto et al., 2010; Liu et al., 2014), PLETHORA (PLT; Kareem et al., 2015), LATERAL ORGAN BOUNDARIES DOMAIN (LBD; Fan et al., 2012), and WOUND INDUCED DEDIFFERENTIATION1 (WIND1; Iwase et al., 2011). The second step is shoot induction from the callus, which consists of several critical events, such as the appropriate distribution of phytohormones, shoot meristem initiation, and organ formation (Cheng et al., 2013; Ikeuchi et al., 2016). One of the most important events in the second step is the induction of the organizing center regulator *WUSCHEL* (*WUS*), which is controlled by the interaction between auxin and cytokinin (Gordon et al., 2007; Cheng et al., 2013). The correct distribution of auxin and cytokinin is essential for *WUS* induction during de novo shoot regeneration (Cheng et al., 2013). Importantly, two recent studies have shown that cytokinin directly activates *WUS* expression by the B-type ARABIDOPSIS RESPONSE REGULATORS (Meng et al., 2017; Zhang et al., 2017).

Shoot regeneration is very valuable in genetic engineering and agricultural applications, but most plant species cannot regenerate shoots from highly differentiated tissues or organs (Birnbaum and Alvarado, 2008). Even in the same species, the shoot regeneration capacity varies among different genotypes (Motte et al., 2014). However, the mechanisms underlying this natural variation in shoot regeneration capacity remain unclear. Several studies have identified a few quantitative trait loci related to natural variations in shoot regeneration (Schiantarelli et al., 2001; Lall et al., 2004; Velázquez et al., 2004). A recent study has shown that the *RECEPTOR-LIKE PROTEIN KINASE1* gene is involved in natural variation in shoot regeneration capacity (Motte et al., 2014). Further identification of the critical genes that control shoot regeneration and how

[1] The work was supported by the National Natural Science Foundation of China (31270231 and 91217308).

[2] These authors contributed equally to the article.

[3] Address correspondence to lixg@sdau.edu.cn or zhangxs@sdau.edu.cn.

The author responsible for distribution of materials integral to the findings presented in this article in accordance with the policy described in the Instructions for Authors (www.plantphysiol.org) is: Xian Sheng Zhang (zhangxs@sdau.edu.cn).

X.S.Z., X.G.L., and H.Z. conceived and designed the experiments; H.Z., T.T.Z., H.L., D.Y.S., M.W., and X.M.B. performed the experiments; X.S.Z. and X.G.L. analyzed data and wrote the article.

[OPEN] Articles can be viewed without a subscription.

www.plantphysiol.org/cgi/doi/10.1104/pp.17.00633

they vary among different genotypes are required for research in both the mechanisms and applications of shoot regeneration.

Reactive oxygen species (ROS) are crucial signaling molecules that can alter their target protein's activity by oxidative posttranslational modifications (Waszczak et al., 2015). Many proteins that act in hormonal signal perception and response, MAPK signal transduction, and the influx channel pathway are redox sensitive to ROS (Waszczak et al., 2015; Kimura et al., 2017). Altered levels of ROS lead to changes in the activity of these target proteins and affect various developmental processes (Schippers et al., 2016). During root development, ROS homeostasis is critical for the transition from cell proliferation to cell differentiation (Tsukagoshi et al., 2010). High levels of ROS result in reduced root meristem activity (Tsukagoshi et al., 2010) and small leaf size (Lu et al., 2014). ROS also is involved in regulating the polar growth of pollen and root hairs (Mangano et al., 2016) and the senescence of leaf and flower (Rogers and Munné-Bosch, 2016). In addition, ROS is generated in various subcellular compartments. Chloroplasts (Dietz et al., 2016), mitochondria (Huang et al., 2016), and peroxisomes (Sandalio and Romero-Puertas, 2015) are the major producers of ROS in plant cells.

ROS homeostasis is governed by diverse antioxidant factors (Considine and Foyer, 2014; Lu and Holmgren, 2014). Thioredoxins (Trxs) are key actors in modulating ROS scavenging, and functional loss of Trx results in altered ROS levels (Dos Santos and Rey, 2006; Schippers et al., 2016). Trxs are widely distributed proteins with a main function to reduce a specific S-S group through the conserved motif CxxC (Gelhaye et al., 2005; Meyer et al., 2005). Trxs alter the activity of interacting target proteins via thiol-based redox modifications (Rouhier et al., 2015). A number of potential Trx targets have been identified using proteomic approaches (Montrichard et al., 2009). Trxs can affect diverse signaling pathways by modulating the activity of their target proteins, such as enzymes of peroxiredoxins and glutathione peroxidase for ROS scavenging (Dos Santos and Rey, 2006), transcription factors for gene expression (Murmu et al., 2010; Viola et al., 2013), and hormonal receptors for signal transduction (Tada et al., 2008). The mitochondrial respiratory chain NADH dehydrogenase complex (Complex I) consists of several essential subunits and is one of the major sites of electron entry into the electron transport chain in the process of ATP production (Braun et al., 2014). An altered redox state of the subunits results in reduced Complex I activity (Galkin et al., 2008). Proteomic analyses have revealed that many subunits of Complex I are potential targets of Trxs, suggesting a crucial role for Trxs in regulating mitochondrial Complex I function (Balmer et al., 2004; Yoshida et al., 2013; Braun et al., 2014; Dröse et al., 2014). However, the evidence that Trxs directly regulate these subunits remains missing. Redox of Trxs regulates diverse developmental processes, such as embryo formation, leaf development, and maintenance of meristem activity (Benitez-Alfonso et al., 2009; Bashandy et al., 2010; Meng et al., 2010). Here, we showed that Trx-dependent redox modification regulated de novo shoot initiation via the modulation of ROS homeostasis. This study provides novel information for understanding the mechanisms of natural variation in plant regeneration.

RESULTS

Loss of Function of *DCC1* Results in the Inhibition of Shoot Regeneration

To determine the function of Trxs in shoot regeneration, seven T-DNA insertion mutants of Trx (Trx O1, Trx O2, Trx H1, Trx H2, Trx H5, AT5G50100, and AT1G52590) from the Arabidopsis Biological Resource Center were screened, but only the *SALK_051222C* (*AT5G50100*) mutant showed severe defects in shoot regeneration (Supplemental Table S1). This mutant contained a T-DNA insert in the fourth intron of *AT5G50100* (Supplemental Fig. S1A). Reverse transcription-PCR analyses showed that the transcript level of this gene was decreased in this mutant (Supplemental Fig. S1B), suggesting that the T-DNA insertion leads to reduced levels of functional transcripts. *AT5G50100* encodes a protein in the thiol-disulfide oxidoreductase family, whose members contain a conserved DxxCxxC motif in their N terminus (Ginalski et al., 2004). In Arabidopsis (*Arabidopsis thaliana*), there exist three members with a DxxCxxC motif, but their functions have not been determined. Thus, *AT5G50100* was designated as *DCC1*.

Loss of function of *DCC1* resulted in a decreased capacity for shoot regeneration, including the low shoot regeneration frequency and the small number of shoots per callus (Fig. 1, A–C). Wild-type callus generated shoots on shoot induction medium (SIM) at 16 d (Fig. 1, A and B), but the *dcc1* mutant callus took 20 d to produce shoots (Fig. 1, A and B). The shoot regeneration frequency in wild-type Columbia-0 (Col-0) was 100% at 28 d on SIM, while that of *dcc1* was about 30% (Fig. 1, A and B). The number of shoots per callus was significantly lower in *dcc1* than in the wild type (Fig. 1, A and C). Furthermore, the phenotypes of the frequencies of shoot regeneration and the shoot number per callus caused by mutation of *DCC1* were both rescued by the transformation of the complementary construct *ProDCC1:DCC1* into the *dcc1* mutant (Fig. 1, A–C). Thus, these results indicate that mutation of *DCC1* leads to an inhibition of shoot regeneration. Furthermore, we showed that *DCC1* was expressed mainly in the inner region of the callus during shoot regeneration by both in situ hybridization (Fig. 1D) and GUS analyses (Fig. 1E).

DCC1 Encodes a Functional Trx Localized in Mitochondria

DCC1 contained an N-terminal DxxCxxC motif in a function-unknown DUF393 domain (in the Pfam database; Fig. 2A). The DxxCxxC motif is a conserved

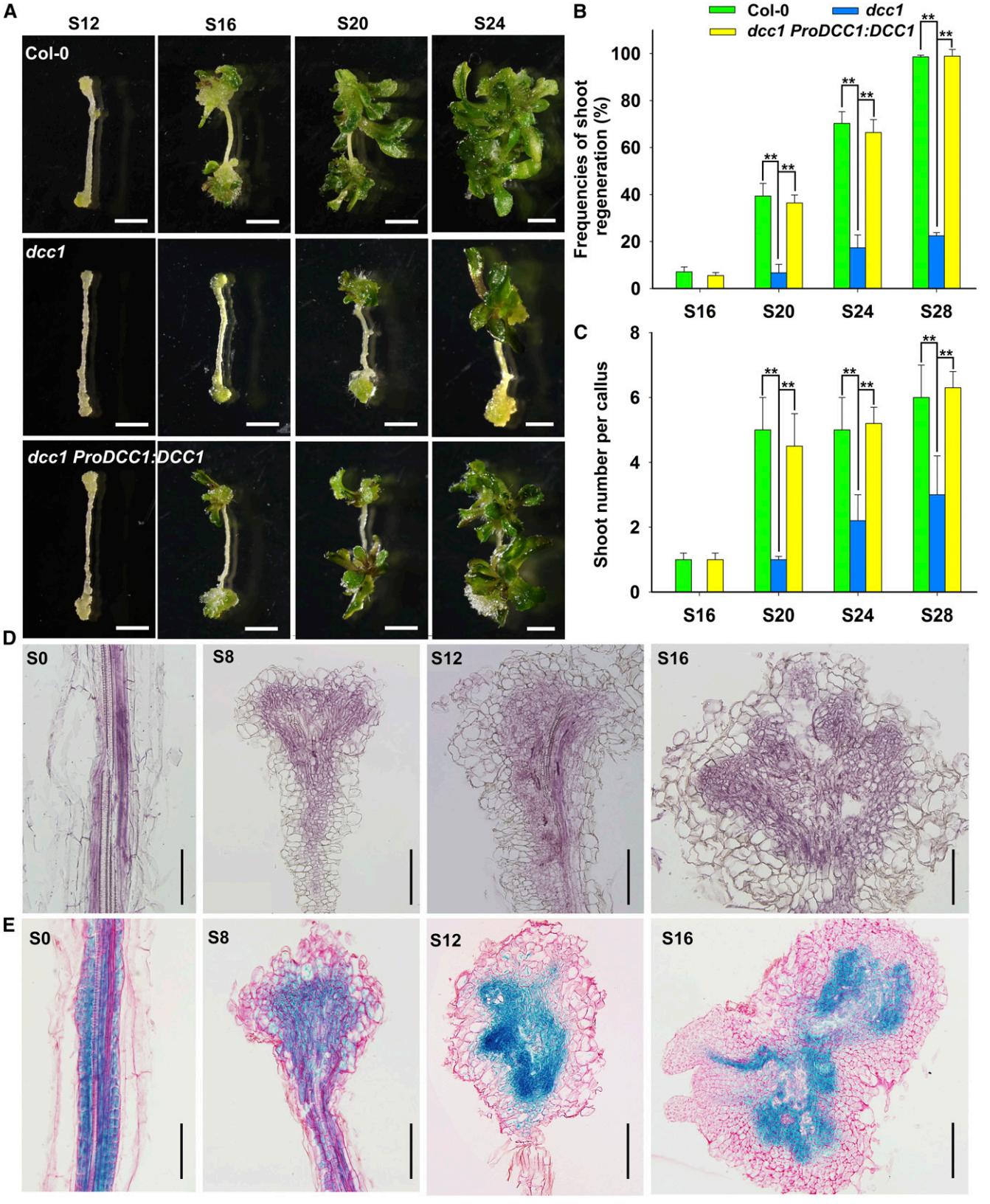

Figure 1. Shoot regeneration is inhibited in the *dcc1* mutant. A to C, Callus morphology (A), frequencies of shoot regeneration from calli (B), and number of shoots per callus (C) in wild-type Col-0, *dcc1*, and *dcc1 ProDCC1*:*DCC1* cultured on SIM at the indicated times. D, Expression pattern of *DCC1* detected by in situ hybridization in calli of Col-0 at the indicated times on SIM.

signature sequence for DCC family proteins in various species, but not in animals (Fig. 2B). Phylogenetic analysis indicated that DCC1 shared high homology with several proteins in species such as *Camelina sativa*, *Brassica rapa*, and *Raphanus sativus* (Fig. 2C). The presence of two Cys residues in the DxxCxxC motif implied a function for DCC1 in regulating thiol-disulfide exchange. Thus, we performed a Trx activity detection assay using fluorescein isothiocyanate-labeled insulin (FiTC-insulin). FiTC-insulin is a highly sensitive substrate for the measurements of Trx activity and displays higher fluorescence after disulfide reduction (Montano et al., 2014). The reduction assay was performed by incubation with purified DCC1 protein, and a high fluorescence intensity was achieved, whereas the control without DCC1 protein showed a low level of insulin reduction (Fig. 2D), confirming its activity as a functional Trx.

DCC1 contained a mitochondrial signal sequence, implying that it might be localized in the mitochondria (Fig. 2A). To test this hypothesis, we obtained a well-established marker line, MT-GK, specially expressing GFP in mitochondria (Mito-GFP; Nelson et al., 2007). Then, the construct *35S:DCC1-RFP* was introduced into the MT-GK line. The roots of the T1 seedlings were used for imaging by laser confocal microscopy. The DCC1-RFP signal was colocalized with the Mito-GFP signal of the control mitochondrion marker (Fig. 2E), indicating that DCC1 is localized in mitochondria.

DCC1 Interacts Directly with CA2

To uncover the functional pathway of DCC1 in shoot regeneration, we searched for its potential target(s). We analyzed the published proteome-wide binary protein-protein interaction map constructed by yeast two-hybrid assay in Arabidopsis and found a DCC1 potential interaction target, CARBONIC ANHYDRASE2 (CA2; Arabidopsis Interactome Mapping Consortium, 2011), which is a β-carbonic anhydrase (Soto et al., 2015). CA2, together with other four carbonic anhydrases (CA1, CA3, CAL1, and CAL2), constitutes a functional subunit of mitochondrial respiratory complex I (Soto et al., 2015). By a yeast two-hybrid assay, we found that only the yeast cotransformed with DCC1-AD and CA2-BD constructs could survive on selection medium (Fig. 3A). In pull-down assays using the purified proteins of DCC1 and CA2, an obvious lane of DCC1-His was observed (Fig. 3B). To further confirm the interaction between DCC1 and CA2 in vivo, we cotransformed the constructs *DCC1-nLUC* and *CA2-cLUC* into *Nicotiana benthamiana* leaves and observed high fluorescence intensity compared with that in the controls (Fig. 3C). In DCC1-GFP immunoprecipitation assays of the F1 generation of the *35S:DCC1-GFP* line crossed with the *35S:CA2-MYC* line, we detected an obvious lane of the CA2-MYC protein (Fig. 3D), indicating an interaction between DCC1 and CA2.

Mutation of *CA2* Causes the Decreased Shoot Regeneration Capacity

To determine the function of *CA2* in shoot regeneration, we obtained the T-DNA insertion mutant *ca2* and analyzed its shoot regeneration capacity. Mutation of *CA2* led to a significantly decreased shoot regeneration capacity. During shoot regeneration, the shoots started to emerge at 16 d on SIM in the wild type, whereas the mutant callus generated shoots at 20 d on SIM (Fig. 4A). The shoot regeneration frequency of the wild type reached 100% at 28 d after transfer of calli onto SIM, while that of *ca2* was only about 40% (Fig. 4B). The number of shoots per callus showed a similar inhibition (Fig. 4C). The frequencies of shoot regeneration and the shoot number per callus were completely rescued by the transformation of the complementary construct *ProCA2:CA2* into the *ca2* mutant (Fig. 4, A–C). Next, we crossed the two single mutants and obtained the homozygous double mutant *dcc1ca2*. The double mutant *dcc1ca2* showed similar phenotypes to those in the *dcc1* mutant in terms of inhibited shoot regeneration (Supplemental Fig. S2, A–C). Furthermore, we detected the spatiotemporal expression patterns of *CA2* and showed that *CA2* expression in the callus started at 8 d on SIM and increased gradually in the inner region of the callus (Fig. 4, D and E).

Mutation of *DCC1* or *CA2* Leads to Reduced Complex I Activity and Increased ROS Level

DCC1 was a functional Trx and interacted directly with CA2 protein, implying that CA2 might be reduced by DCC1. Therefore, we performed a reduction assay by using purified recombinant CA2 protein as the substrate. CA2 was incubated with or without GST-cleaved recombinant DCC1 protein. DTT (0.3 mM) was added to recycle DCC1 activity. The reduction of CA2 was monitored by the mobility shift in nonreducing SDS-PAGE. CA2 contained two Cys residues (Cys-83 and Cys-137) and formed dimer and oligomer complexes by intermolecular disulfide bonds (Fig. 5, A and

Figure 1. (*Continued.*)
E, Expression pattern of *DCC1* detected by GUS staining in calli of *ProDCC1:DCC1-GUS* transgenetic lines at the indicated times on SIM. S0 represents calli cultured on callus induction medium (CIM) at 6 d using roots as explants before transfer to SIM. S8, S12, S16, S20, S24, and S28 indicate calli cultured on SIM at 8, 12, 16, 20, 24, and 28 d, respectively. SE values were calculated from three sets of biological replicates, and more than 100 calli were examined in each replicate. Asterisks indicate significant differences: **, $P < 0.01$ (Student's one-tailed *t* test). Bars = 500 μm.

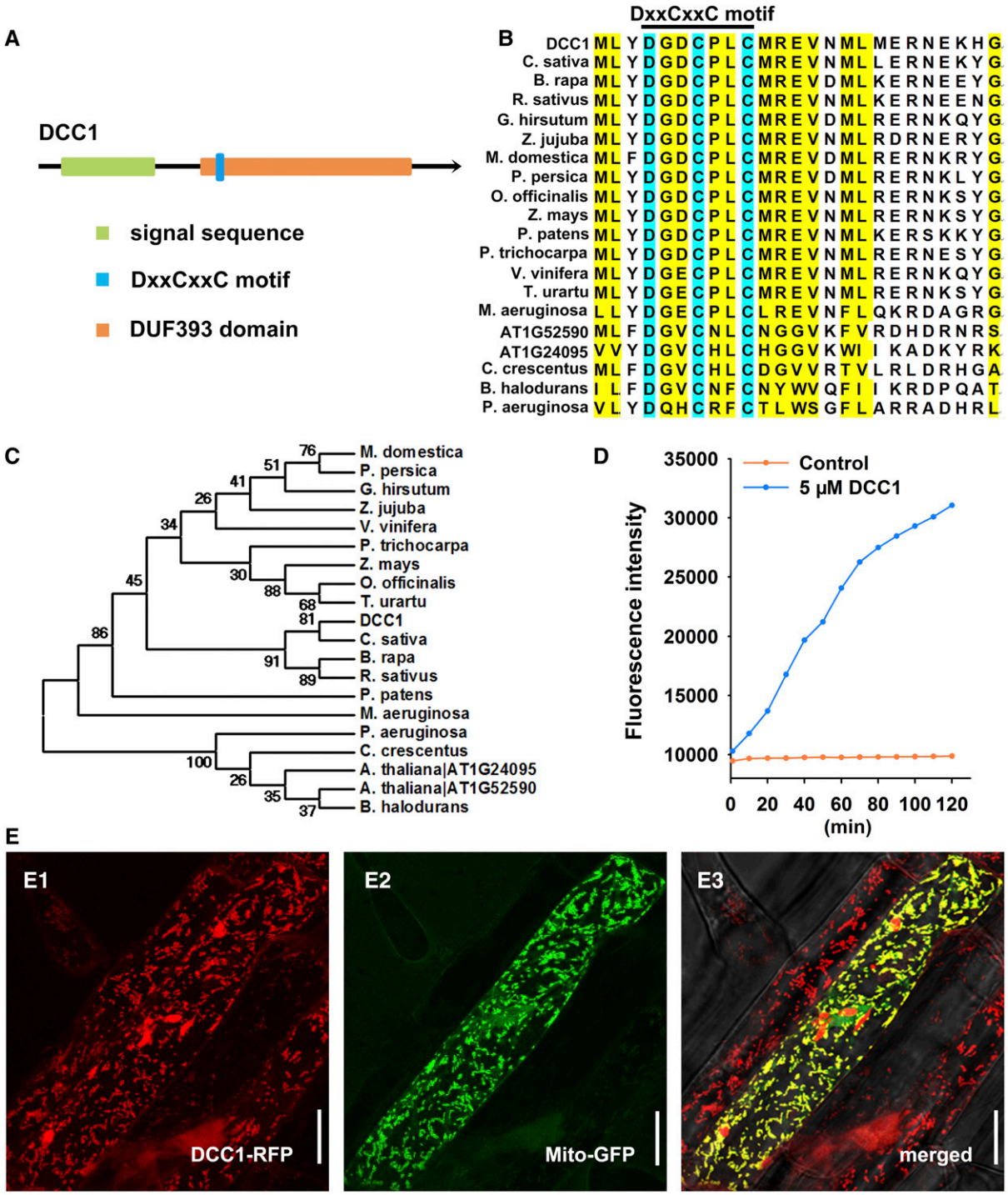

Figure 2. DCC1 is a functional Trx localized in mitochondria. A, Model of the DCC1 protein with a mitochondria signal sequence predicted in the UniProt database and a conserved DxxCxxC motif in a function-unknown DUF393 domain analyzed in the Pfam database. B, Alignment of the amino acid sequences of different DCC family proteins. The DxxCxxC motif is a conserved signature sequence for DCC family proteins in various species. The National Center for Biotechnology Information accession numbers of proteins in different species are presented in "Materials and Methods." C, Phylogenetic analyses of DCC1 with its homologs in various species. DCC1 shares high homology with several proteins in species such as *C. sativa*, *B. rapa*, and *R. sativus*. D, Insulin reduction by recombinant DCC1 proteins. Purified DCC1 proteins were subjected to a reduction assay by using FiTC-insulin as the substrate, which displayed higher fluorescence after disulfide reduction. The assay mixture lacking recombinant DCC1 proteins served as the control. Fluorescence intensity was recorded at 515- to 525-nm emission after 480- to 495-nm excitation for 120 min in a fluorescent plate reader at room temperature. E, Subcellular localization of DCC1. MT-GK is a

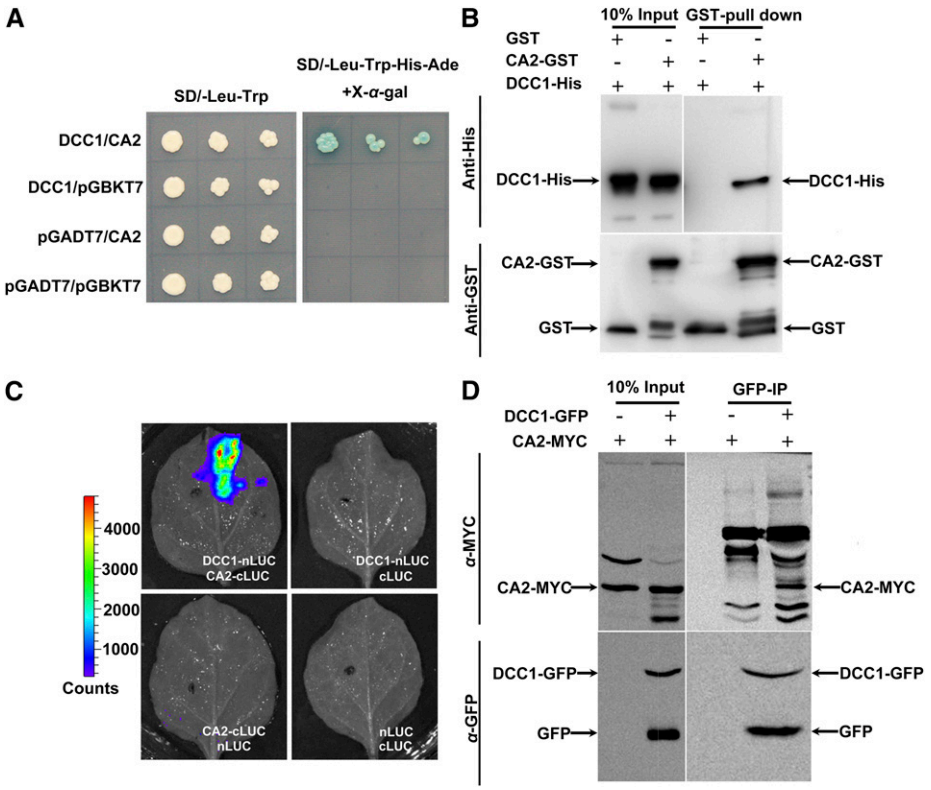

Figure 3. DCC1 interacts with CA2. A, Interaction between DCC1 and CA2 in the yeast two-hybrid assay. Activation was observed at 3 d on selection plates (synthetic dextrose [SD]-Leu-Trp-His-Ade) with X-α-gal. B, Interaction between DCC1 and CA2 in the pull-down assay. The 10% input and GST pull-down proteins were detected by immunoblotting using anti-His antibody (top row). CA2-GST and GST proteins were detected by immunoblotting using anti-GST antibody (bottom row). C, Interaction between DCC1 and CA2 in firefly luciferase complementation assays in transiently transfected leaf of *N. benthamiana*. D, Interaction between DCC1 and CA2 in coimmunoprecipitation assays. The 10% input and immunoprecipitated proteins with anti-GFP (GFP-IP) were detected by immunoblotting using an anti-MYC antibody (top row). The 10% input and DCC1-GFP proteins were detected by immunoblotting using an anti-GFP antibody (bottom row).

B). The intensity of CA2 complex lanes was decreased significantly after incubation with DCC1 protein (Fig. 5, A and B), suggesting that DCC1 promotes monomer formation by reduction of the CA2 complex.

CA2 is a key subunit of the mitochondrial respiratory complex I, and defect in *CA2* leads to decreased activity of complex I (Soto et al., 2015). Thus, we detected the activity of respiratory complex I in *dcc1*, *ca2*, and *dcc1ca2* during shoot regeneration. Functional loss of *DCC1* or *CA2* caused a significantly decreased activity of the mitochondrial respiratory complex I (Fig. 5C). The complex I activity in the double mutant *dcc1ca2* was not more affected than that in the single mutants, indicating that both proteins act in the same pathway. Furthermore, the reduced activity of complex I in the *dcc1ca2* double mutant was completely rescued by the addition of both of DCC1 and CA2 proteins but not by the addition of only DCC1 or CA2 (Fig. 5D). These results suggest that DCC1 affects complex I activity via redox regulation of CA2 protein. A previous study has shown that the impaired activity of respiratory complex I results in increased ROS levels (Soto et al., 2015). Thus, we hypothesize that the reduced mitochondrial respiratory complex I activity triggers mitochondrial ROS production. To test this hypothesis, we performed 3,3′-diaminobenzidine (DAB) staining assays to detect the ROS levels in callus (Xie et al., 2014). During shoot regeneration, functional loss of *DCC1* or *CA2* resulted in increased ROS levels in calli cultured on CIM or SIM, respectively (Fig. 6). The ROS level in the double mutant *dcc1ca2* was consistent with that in either single mutant (Fig. 6).

ROS Levels Mediate the Inhibition of Shoot Regeneration

Since the loss of function of *DCC1* and *CA2* resulted in increased ROS levels, we thought that the inhibition of shoot regeneration in the *dcc1* or *ca2* mutant might be due to increased ROS levels. To test this hypothesis, we treated explants of the wild type with exogenous H_2O_2, a well-demonstrated regent responsible for increasing ROS levels (Yu et al., 2016), and found that shoot regeneration was inhibited significantly in the treated

Figure 2. (*Continued.*)
well-established marker line specially expressing Mito-GFP. The construct *35S:DCC1-RFP* was transformed into MT-GK. The T1 transgenetic line roots were excised for imaging by a confocal microscope. The DCC1-RFP signal (E1) was observed at 505- to 550-nm emission after 561-nm excitation, whereas the Mito-GFP signal (E2) was observed at 570- to 620-nm emission after 488-nm excitation. The merged signals of GFP and RFP showed yellow color (E3), indicating that DCC1 is localized in the mitochondria. Bars = 20 μm.

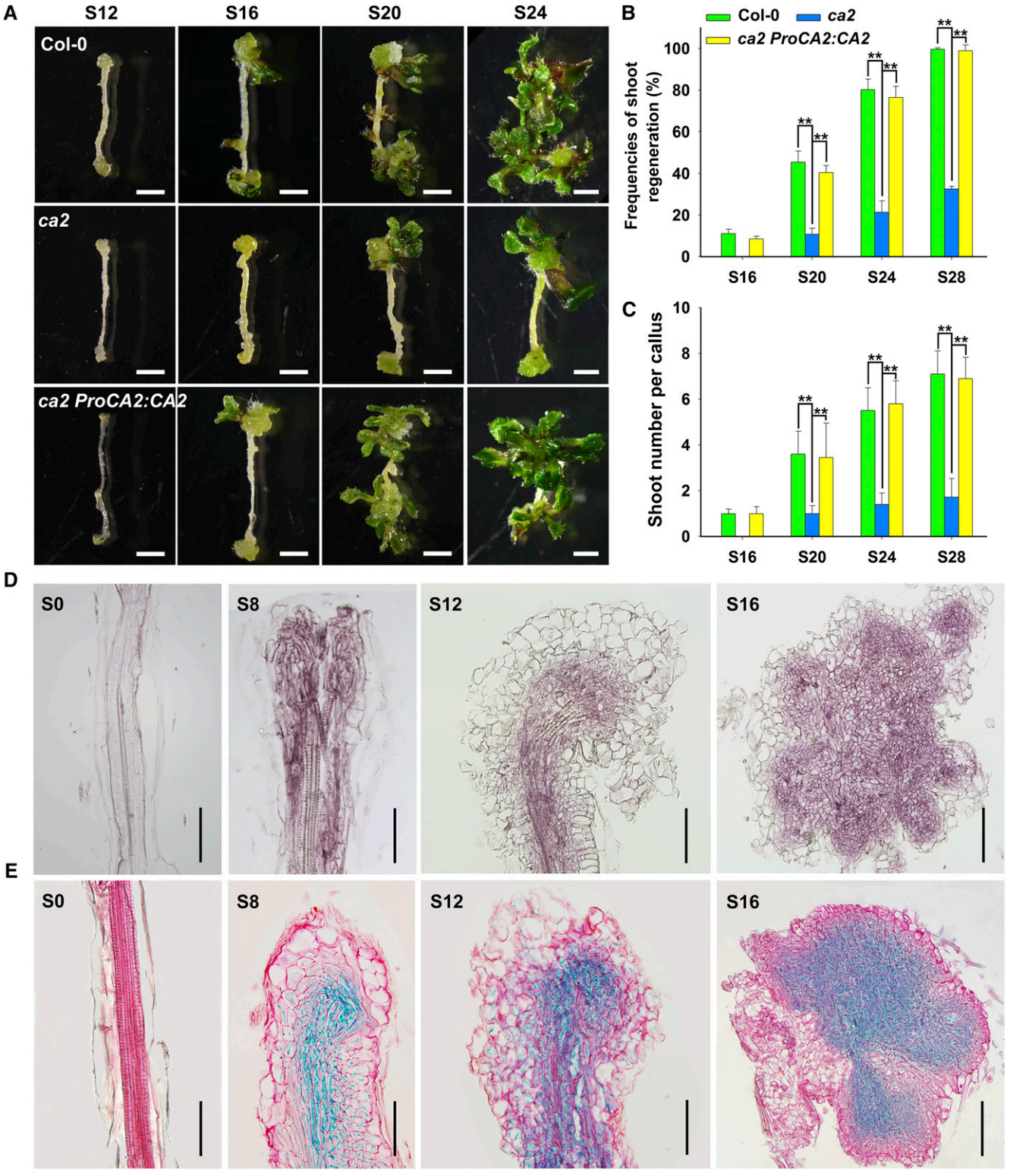

Figure 4. Loss of function of *CA2* caused the decreased capacity of shoot regeneration. A to C, Callus morphology (A), frequencies of shoot regeneration from calli (B), and number of shoots per callus (C) in wild-type Col-0, *ca2*, and *ca2 ProCA2*:*CA2* cultured on SIM at the indicated times. D, Expression pattern of *CA2* detected by in situ hybridization in calli of Col-0 at the indicated times on SIM. E, Expression pattern of *CA2* detected by GUS staining in calli of *ProCA2*:*CA2-GUS* transgenetic lines at the indicated times on SIM. S0 represents calli cultured on CIM at 6 d using roots as explants before transfer to SIM. S8, S12, S16, S20, S24, and S28 indicate calli cultured on SIM at 8, 12, 16, 20, 24, and 28 d, respectively. SE values were calculated from three sets of biological replicates, and more than 100 calli were examined in each replicate. Asterisks indicate significant differences: **, $P < 0.01$ (Student's one-tailed *t* test). Bars = 500 μm.

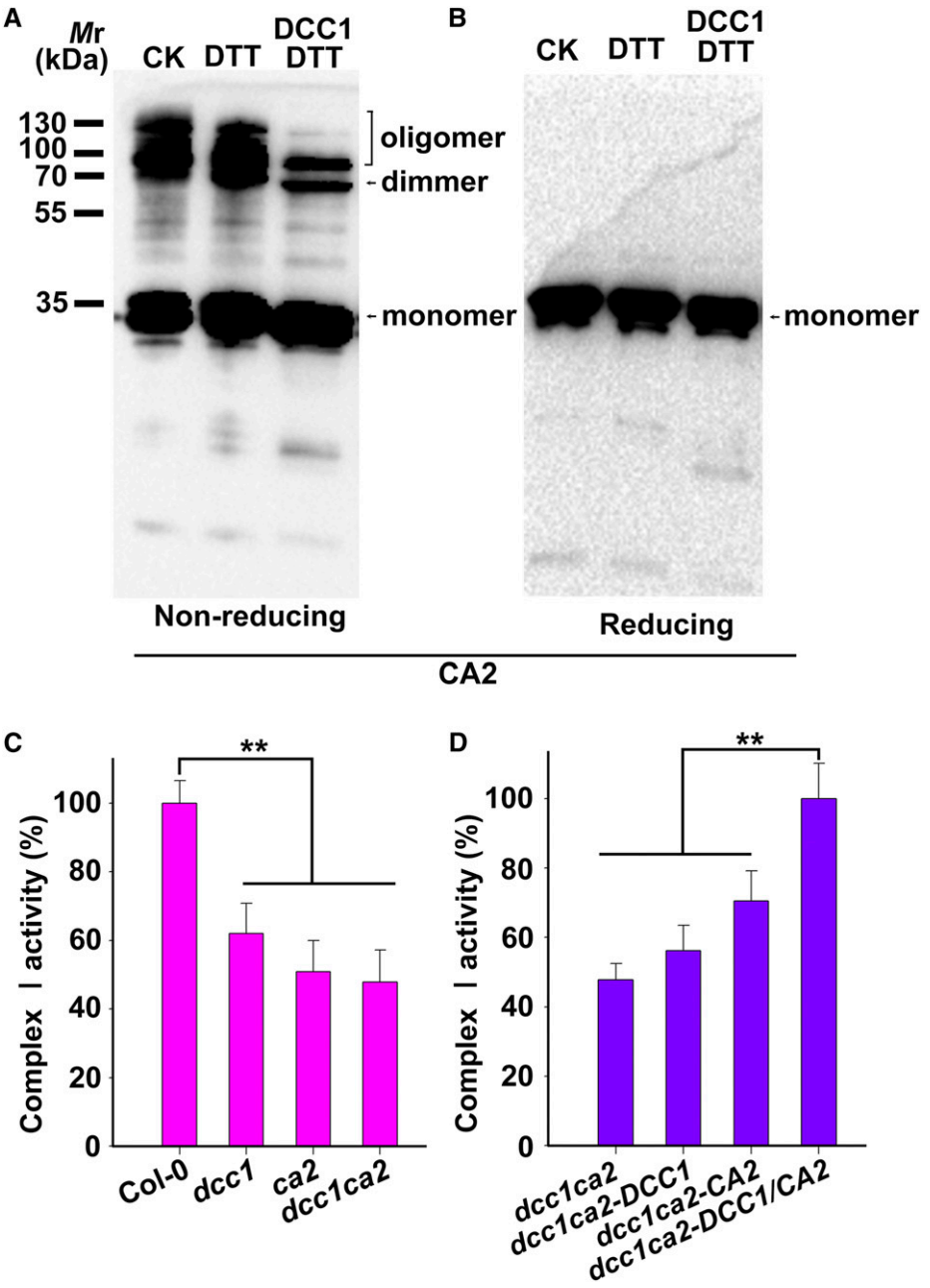

Figure 5. DCC1 regulates Complex I activity via CA2 protein. A and B, CA2 dimer and oligomer were reduced by DCC1. Purified CA2-His protein was incubated in the assay mixture with or without DCC1 GST-cleaved protein (5 μM) for 30 min at room temperature and then subjected to nonreducing (A) or reducing (B) SDS-PAGE followed by immunoblot analysis. DTT (0.3 mM) was added to recycle DCC1 Trx activity. The positions of the monomer, dimer, and oligomer of CA2 are indicated. CA2 dimer and oligomer showed significantly reduced levels when incubated with DCC1 proteins (right lane). The reaction mixture without DCC1 proteins was used as the control (left and middle lanes). CK, Control check. C, Relative activity of mitochondrial respiratory Complex I. Mitochondria were isolated from calli (0.1 g) of wild-type Col-0, *dcc1*, *ca2*, and *dcc1ca2* cultured on SIM at 16 d. Mitochondrial proteins (20 μg) were used to determine the Complex I activity. The absorbance of all samples was measured at 340 nm for 60 min using a plate reader. Complex I activity was calculated from the decrease in absorbance per minute. Functional loss of DCC1 or CA2 resulted in reduced activity of Complex I. D, Relative activity of Complex I in calli of *dcc1ca2* after the addition of recombinant CA2 or DCC1 protein. Purified CA2-His proteins and DCC1-His proteins were added to the assay mixture. Only the addition of both DCC1 and CA2 proteins completely rescued the reduced Complex I activity. Asterisks indicate significant differences: **, $P < 0.01$ (Student's one-tailed *t* test).

explants (Fig. 7). Moreover, higher levels of H_2O_2 led to lower shoot regeneration capacities (Fig. 7). The wild type without H_2O_2 treatment generated visible shoots at 16 d on SIM, whereas the wild type treated with 0.005‰ H_2O_2 and 0.01‰ H_2O_2 generated shoots at 20 d on SIM (Fig. 7A). At 28 d on SIM, the wild type without H_2O_2 treatment had a shoot regeneration frequency of 100% (Fig. 7B), whereas the wild type treated with 0.005‰ H_2O_2 and 0.01‰ H_2O_2 had shoot regeneration frequencies of 70% and 30%, respectively (Fig. 7B). The number of shoots regenerated from wild-type calli also was decreased when treated with exogenous H_2O_2 (Fig. 7C), indicating that ROS inhibits shoot regeneration.

Next, we determined whether GSH, the main endogenous antioxidant responsible for ROS removal (Lu and Holmgren, 2014), could rescue the phenotypes of *dcc1* and *ca2* by decreasing the ROS levels. The frequencies of shoot regeneration in the *dcc1*, *ca2*, and *dcc1ca2* mutants were increased with gradually increasing concentrations of GSH (Supplemental Fig. S3A). The number of shoots per callus showed similar increases under GSH treatment (Supplemental Fig. S3B). The *dcc1*, *ca2*, and *dcc1ca2* mutants were completely rescued by GSH at 600 μM (Fig. 8). Although shoot regeneration was promoted in the wild type by GSH, the shoot regeneration in the *dcc1*, *ca2*, and *dcc1ca2* mutants by GSH was increased significantly compared

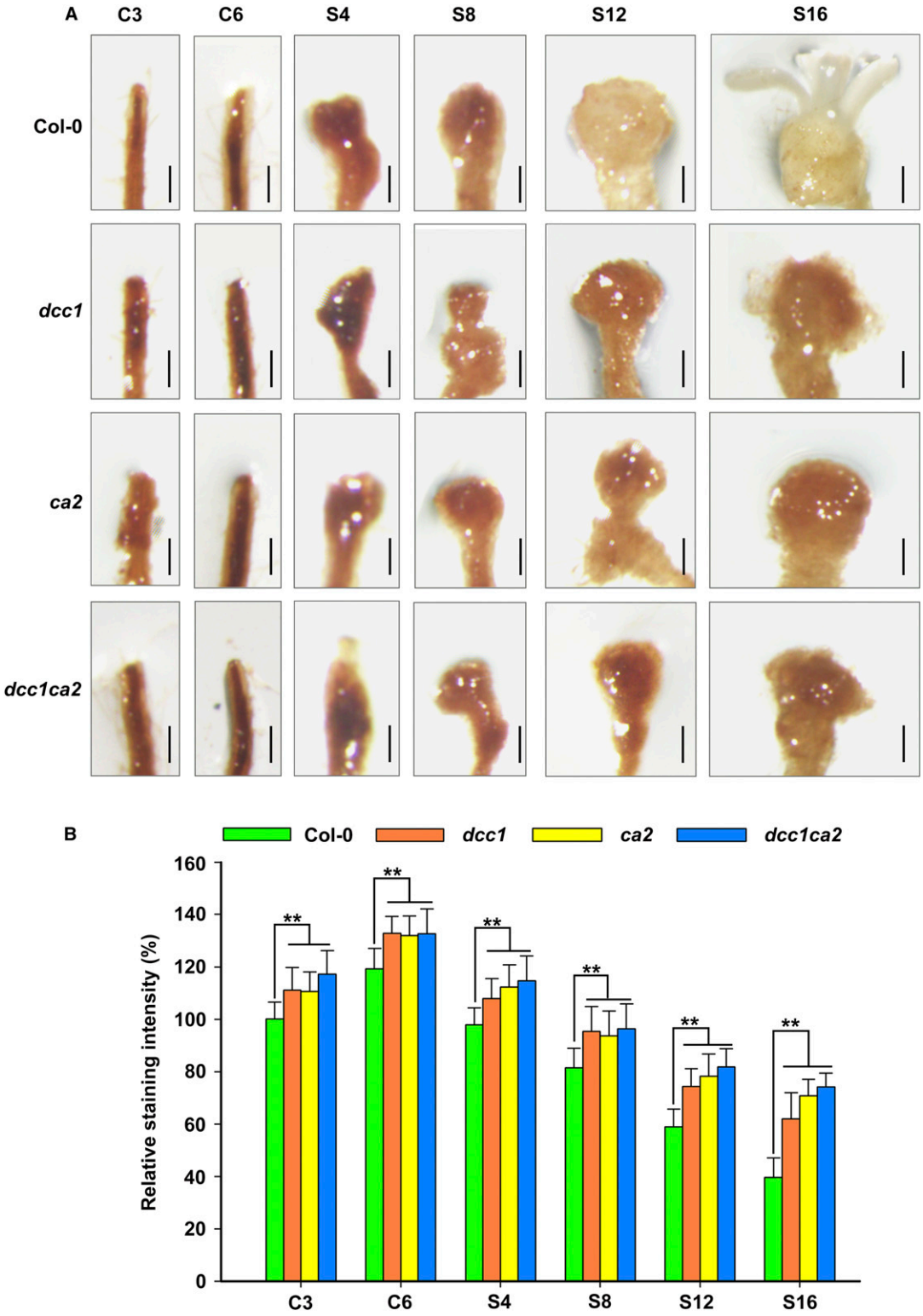

Figure 6. Mutation of *DCC1* or *CA2* results in increased ROS levels. A, Levels of ROS in calli of Col-0, *dcc1*, *ca2*, and *dcc1ca2* on CIM and SIM at the indicated times by DAB staining. B, Relative ROS staining intensity in calli of wild-type Col-0, *dcc1*, *ca2*, and *dcc1ca2* on CIM and SIM at the indicated times. C3 and C6 indicate calli cultured on CIM at 3 and 6 d, respectively. S4, S8, S12, and S16 indicate calli cultured on SIM at 4, 8, 12, and 16 d, respectively. SE values were calculated from three sets of biological replicates, and more than 100 calli were examined in each replicate. Asterisks indicate significant differences: **, $P < 0.01$ (Student's one-tailed *t* test). Bars = 500 μm.

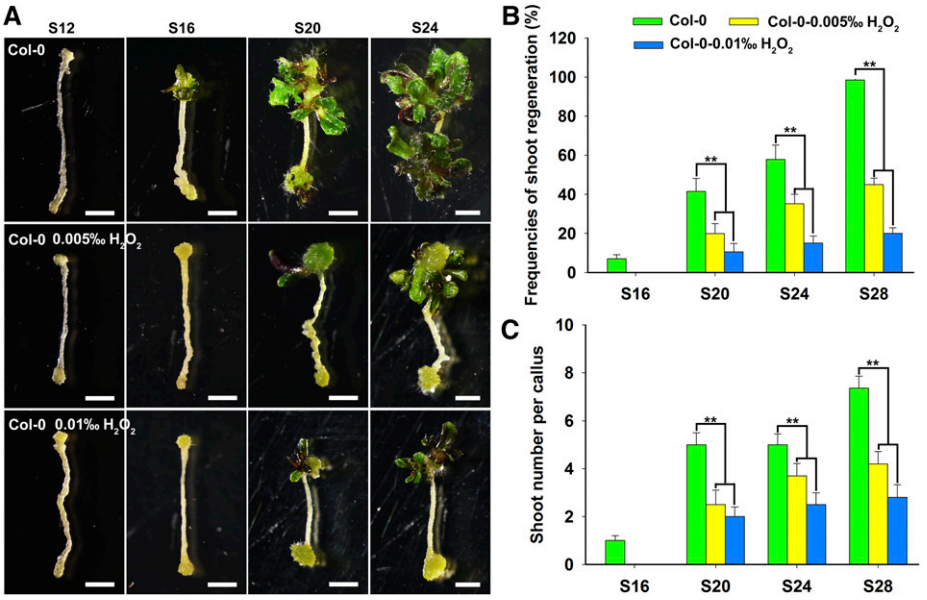

Figure 7. Treatment with exogenous ROS inhibits shoot regeneration. Callus morphology (A), frequencies of shoot regeneration from calli (B), and number of shoots per callus (C) in wild-type Col-0 after treatment with H_2O_2 at different concentrations during shoot regeneration are shown. S12, S16, S20, S24, and S28 indicate calli cultured on SIM at 12, 16, 20, 24, and 28 d, respectively. SE values were calculated from three sets of biological replicates, and more than 100 calli were examined in each replicate. Asterisks indicate significant differences: **, $P < 0.01$ (Student's one-tailed *t* test). Bars = 500 μm.

with that in the wild type (Fig. 8). These results indicate that the reduction of ROS levels by GSH promotes shoot regeneration. To further confirm the function of ROS in shoot regeneration, we transformed the construct *pER8-CAT3*, which overexpressed *CATALASE3* (*CAT3*) when induced with estradiol, into Col-0 and the *dcc1*, *ca2*, and *dcc1ca2* mutants. *CAT3* encodes a catalase that catalyzes the breakdown of H_2O_2 into water and oxygen, thereby reducing the H_2O_2 level (Zou et al., 2015). The *CAT3* overexpression transgenic lines were obtained in the backgrounds of Col-0, *dcc1*, *ca2*, and *dcc1ca2* (Supplemental Fig. S4). The shoot regeneration frequencies and number of shoots per callus were increased in the *CAT3*-overexpressing transgenic lines (Fig. 8), indicating that the reduction in ROS levels by overexpression of *CAT3* rescued the phenotypes of the mutants. *CAT3* overexpression in Col-0 led to about two more shoots per callus than Col-0, whereas *CAT3* overexpression in *dcc1*, *ca2*, and *dcc1ca2* mutants showed about five more shoots compared with their mutants. Thus, these results confirm that the ROS level is critical for regulating the shoot regeneration capacity.

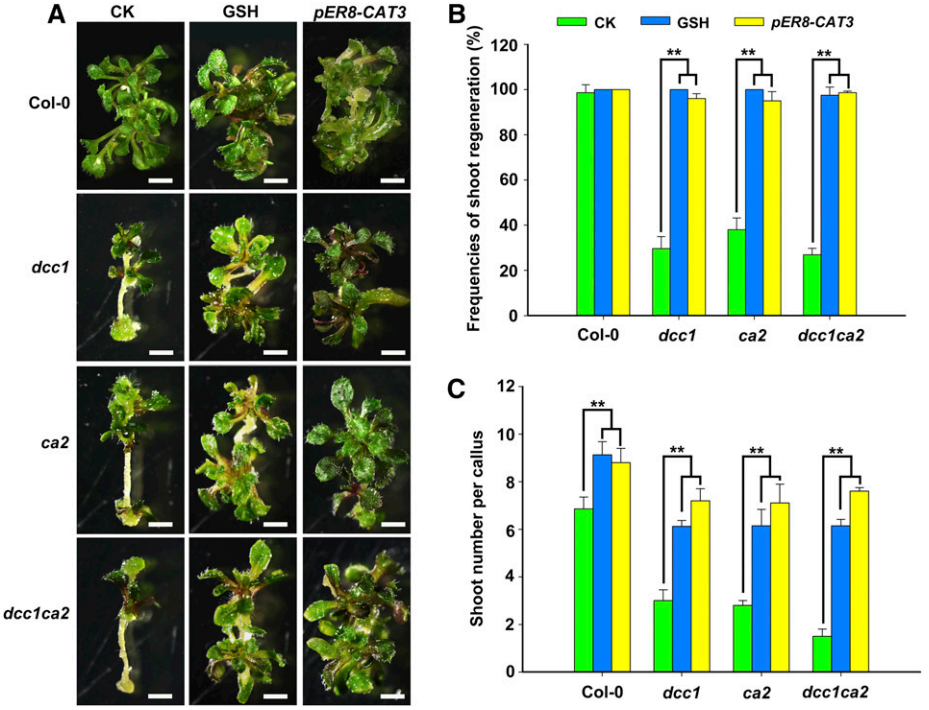

Figure 8. Decreased ROS level rescues phenotypes of the *dcc1ca2* double mutant. Callus morphology (A), frequencies of shoot regeneration from calli (B), and number of shoots per callus (C) in wild-type Col-0, *dcc1*, *ca2*, and *dcc1ca2* after treatment with GSH (600 μM) or overexpression of *CAT3* on SIM at 28 d are shown. GSH is the main endogenous antioxidant responsible for ROS removal. *CAT3* encodes a catalase that catalyzes the breakdown of H_2O_2 into water and oxygen, thereby reducing the H_2O_2 level. CK, Control check. *pER8-CAT3* represents the overexpression of *CAT3* in the *dcc1*, *ca2*, and *dcc1ca2* backgrounds when induced with estradiol. SE values were calculated from three sets of biological replicates, and more than 100 calli were examined in each replicate. Asterisks indicate significant differences: **, $P < 0.01$ (Student's one-tailed *t* test). Bars = 500 μm.

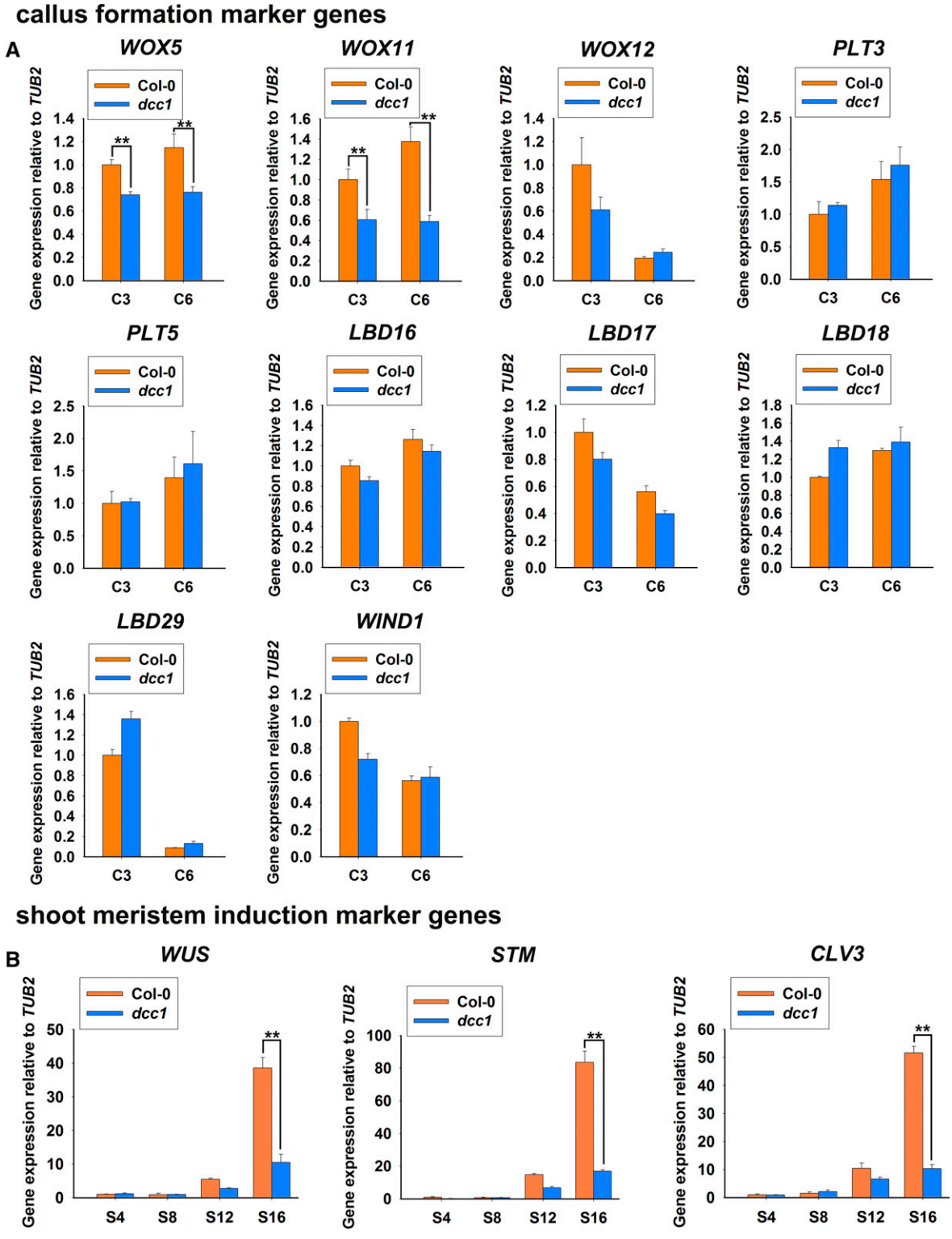

Figure 9. Transcript levels of master genes involved in shoot regeneration. Transcript levels of master genes for callus formation (A) and shoot meristem induction (B) during shoot regeneration are shown. C3 and C6 represent calli cultured on CIM at 3 and 6 d, respectively, using roots as explants before transfer to SIM. S4, S8, S12, and S16 indicate calli cultured on SIM at 4, 8, 12, and 16 d, respectively. SE values were calculated from three sets of biological replicates. Asterisks indicate significant differences: **, $P < 0.01$ (Student's one-tailed *t* test).

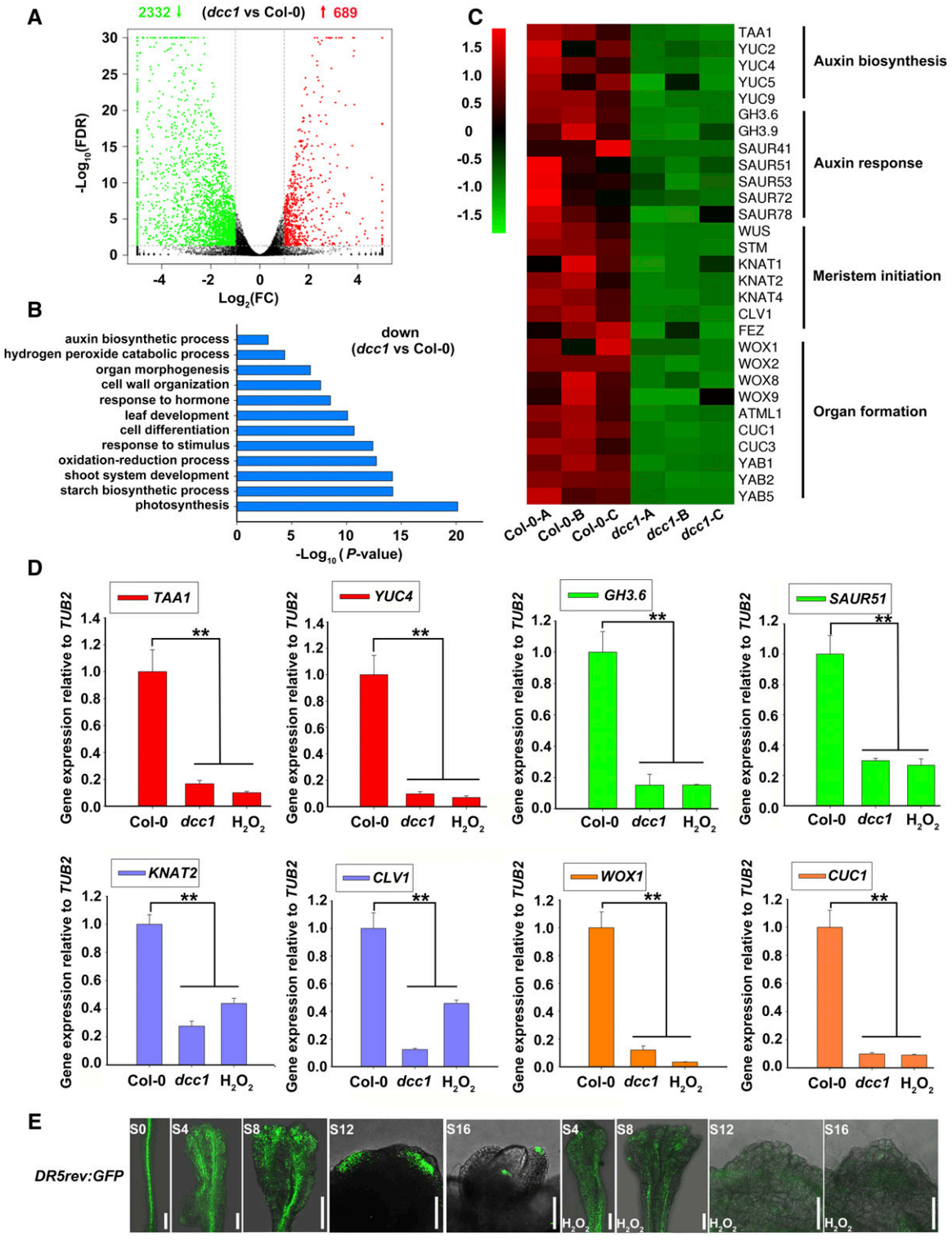

Figure 10. DCC1 regulates shoot regeneration through modulating multiple signaling by RNA-seq analyses. A, Differential gene expression detected by edgeR. A 2-fold change in gene transcript levels between wild-type Col-0 and the mutant *dcc1* with an adjusted *P* value (FDR) cutoff of 0.05 was considered as differential expression: 2,332 genes were down-regulated and 689 genes were up-regulated in the *dcc1* mutant. B, GO analyses of down-regulated genes in the *dcc1* mutant. C, Cluster analysis of transcript levels of genes involved in auxin signaling, meristem initiation, and organ formation. Col-0-A, Col-0-B, and Col-0-C are three repeats of Col-0, and *dcc1*-A, *dcc1*-B, and *dcc1*-C are three repeats of *dcc1*. D, Transcript levels of *TAA1*, *YUC4*, *GH3.6*, *SAUR51*, *KNAT2*, *CLV1*, *WOX1*, and *CUC1* in calli of Col-0, *dcc1*, and H_2O_2 (wild-type Col-0 treated with 0.01‰ H_2O_2 during

ROS Regulates Shoot Regeneration by Modulating Multiple Pathways

Shoot regeneration includes callus formation and shoot meristem induction. To determine whether ROS was involved in the regulation of callus formation by master regulators, we analyzed the expression of *WOXs*, *PLTs*, *LBDs*, and *WIND1* during this process. Only *WOX5* and *WOX11* showed reduced levels in the *dcc1* mutant (Fig. 9A), suggesting that ROS affects callus formation by the modulation of *WOX5* and *WOX11* expression. Next, we detected *WUS*, *SHOOT MERISTEMLESS* (*STM*), and *CLAVATA3* (*CLV3*), which are involved in shoot meristem induction (Ikeuchi et al., 2016). The transcript levels of all three of these genes were decreased in the *dcc1* mutant cultured on SIM at 12 and 16 d (Fig. 9B), suggesting that ROS regulates shoot induction by modulating the expression of *WOXs*, *WUS*, *CLV3*, and *STM*.

To uncover the functional pathways of ROS in detail, we performed an RNA-seq analysis using the calli of wild-type Col-0 and *dcc1* cultured on SIM at 16 d. Three high-quality biological repeats of the wild type (Col-0-A, Col-0-B, and Col-0-C) and *dcc1* (*dcc1*-A, *dcc1*-B, and *dcc1*-C) were used for RNA-seq analyses (Supplemental Fig. S5). Using a 2-fold change in the gene transcript levels between wild-type Col-0 and the mutant *dcc1* with an adjusted *P* value (false discovery rate [FDR]) cutoff of 0.05 as the criterion for differential expression, we identified many differentially expressed genes (Fig. 10A). Among them, 689 genes were up-regulated and 2,332 genes were down-regulated in *dcc1* (Fig. 10A; Supplemental Tables S2 and S3). Gene Ontology (GO) analyses showed that *DCC1* regulated multiple processes, such as auxin biosynthetic process ($P = 1.38 \times 10^{-3}$), shoot system development ($P = 6.33 \times 10^{-15}$), oxidation-reduction process ($P = 1.83 \times 10^{-13}$), cell differentiation ($P = 1.98 \times 10^{-11}$), response to hormones ($P = 2.88 \times 10^{-9}$), cell wall organization ($P = 2.24 \times 10^{-8}$), organ morphogenesis ($P = 1.94 \times 10^{-7}$), and H_2O_2 catabolic process ($P = 4.35 \times 10^{-5}$; Fig. 10B). In addition to *WUS* and *STM*, the meristem master genes *KNOTTED-LIKE FROM ARABIDOPSIS THALIANA1* (*KNAT1*), *KNAT2*, and *KNAT4* (Scofield et al., 2007), *WOXs* (van der Graaff et al., 2009), and *CUP-SHAPED COTYLEDON* (*CUCs*; Ikeuchi et al., 2016) were down-regulated in *dcc1* (Fig. 10, B and C). Next, we performed quantitative reverse transcription (qRT)-PCR to confirm the transcript levels of genes identified in the RNA-seq analyses. As expected, the transcript levels of these genes were low in the *dcc1* mutant and in the presence of exogenous H_2O_2 (Fig. 10D; Supplemental Fig. S6). These results suggest that the DCC1-mediated ROS level regulates shoot regeneration by the genes involved in shoot meristem initiation.

Interestingly, several auxin biosynthetic genes, including *TRYPTOPHAN AMINOTRANSFERASE OF ARABIDOPSIS1* (*TAA1*), *YUCCA2* (*YUC2*), *YUC4*, *YUC5*, and *YUC9* (Zhao, 2010), were significantly down-regulated in *dcc1* (Fig. 10, C and D; Supplemental Fig. S6). The transcript levels of auxin response genes, such as *GRETCHEN HAGEN3.6* (*GH3.6*) and *SMALL AUXIN UPREGULATED51* (*SAUR51*; Hagen and Guilfoyle, 2002; Staswick et al., 2005), also were decreased in *dcc1* (Fig. 10, C and D; Supplemental Fig. S6). Furthermore, we used the well-demonstrated auxin marker *DR5rev*:*GFP* to detect the auxin response signal distribution in regenerating shoots (Cheng et al., 2013). The GFP signal was weakened by H_2O_2 treatment during shoot regeneration (Fig. 10E). Auxin is a critical determinant in shoot regeneration, and the impaired auxin biosynthesis and signaling repress shoot regeneration (Gordon et al., 2007; Cheng et al., 2013). Moreover, the functional loss of *DCC1* led to increased ROS levels (Fig. 6, A and B), and ROS repressed auxin signaling (Fig. 10E). Thus, we propose that the DCC1-mediated ROS level regulates shoot regeneration, at least in part, through a modulation of the auxin biosynthesis and signaling pathway.

DCC1 Is a Major Determinant of Natural Variation in Shoot Regeneration

To determine whether *DCC1* was a factor in the natural variation in shoot regeneration, 48 ecotypes of Arabidopsis were used in shoot regeneration analyses using the roots as explants. The shoot regeneration capacity varied widely among the different ecotypes of Arabidopsis. The shoot regeneration frequencies ranged from 5% to 100% (Supplemental Fig. S7A). The ecotypes Gu-0, Nc-1, Wa-1, and Kelsterbach-4 showed very low shoot regeneration frequencies on SIM at 28 d, while the ecotypes Col-0, Ws-0, Pu2-7, Lan-0, and Bu-0 showed high shoot regeneration frequencies (Supplemental Fig. S7A). These diverse frequencies indicated the wide natural variation in regeneration capacity among Arabidopsis genotypes. There was also a wide range among genotypes in the number of shoots per callus (Supplemental Fig. S7B). Each callus of Col-0, Ws-0, Pu2-7, Bu-0, Tsu-1, and Ct-1 generated more than five shoots, while calli of other ecotypes generated four or fewer. These results confirm that there are diverse shoot regeneration capacities among different ecotypes of Arabidopsis.

Figure 10. (*Continued.*)
shoot regeneration) on SIM at 16 d, as determined by qRT-PCR. *TUBULIN2* (*TUB2*) was the reference gene. Asterisks indicate significant differences: **, $P < 0.01$ (Student's one-tailed *t* test). E, Response patterns of *DR5rev*:*GFP* in calli with or without H_2O_2 treatment on SIM at the indicated times. S0 represents calli cultured on CIM at 6 d using roots as explants before transfer to SIM. S4, S8, S12, and S16 indicate calli cultured on SIM at 4, 8, 12, and 16 d, respectively. Bars = 500 μm.

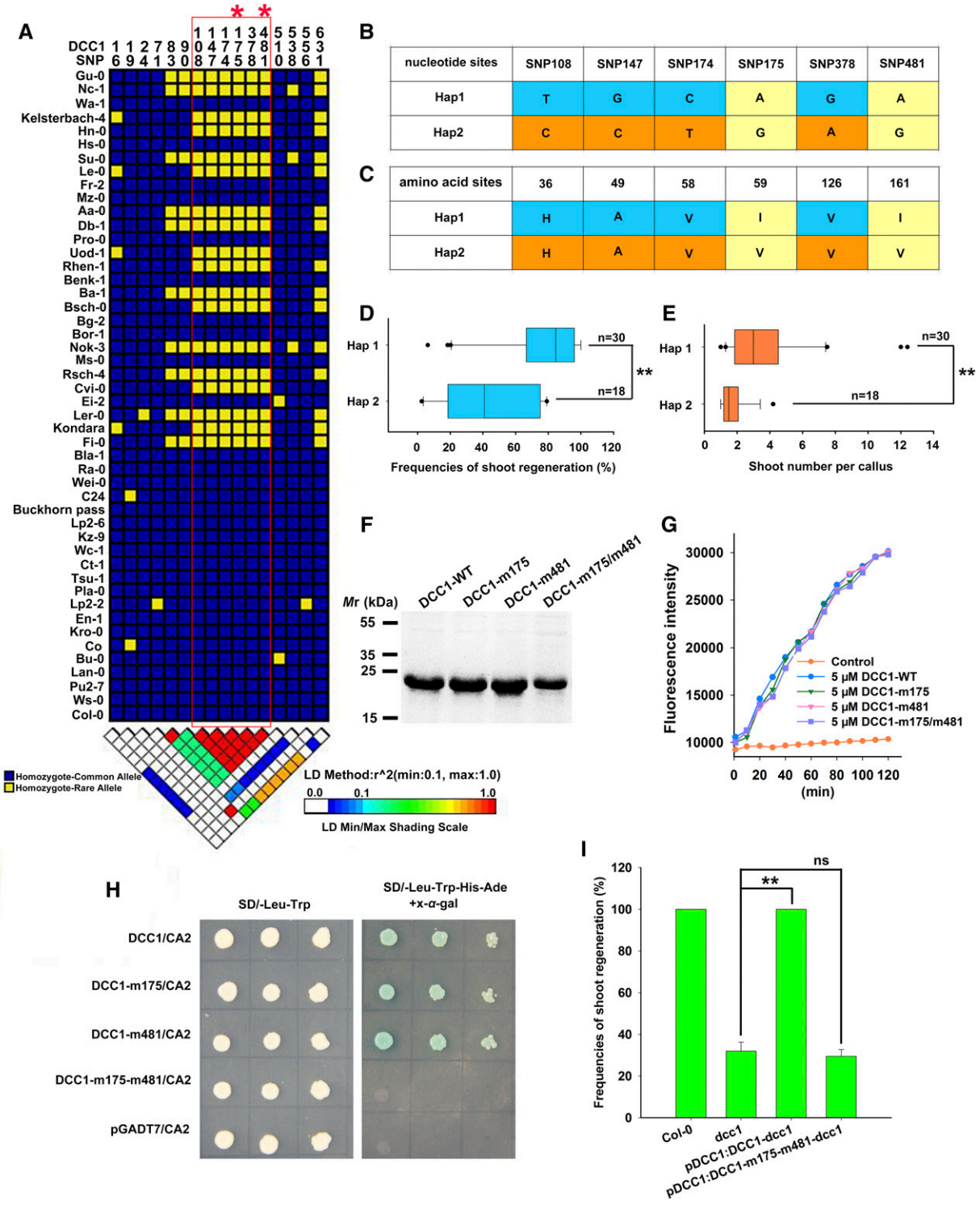

nucleotide sites	SNP108	SNP147	SNP174	SNP175	SNP378	SNP481
Hap1	T	G	C	A	G	A
Hap2	C	C	T	G	A	G

amino acid sites	36	49	58	59	126	161
Hap1	H	A	V	I	V	I
Hap2	H	A	V	V	V	V

Figure 11. DCC1 regulates the capacity of shoot regeneration among different Arabidopsis ecotypes. A, Linkage disequilibrium analyses of *DCC1* in 48 Arabidopsis ecotypes indicated six critical SNPs (SNP 108, 147, 174, 175, 378, and 481). B, Two haplotypes (Hap1 and Hap2) of *DCC1* were characterized based on six SNPs of nucleotide sequences in Arabidopsis natural variants. C, Amino acid sequences of Hap1 and Hap2. Two SNPs (SNP 175 and 481) resulted in amino acid mutations (I59V and I161V). D and E, Shoot regeneration frequencies from calli (D) and number of shoots per callus (E) in each haplotype group (n, number of genotypes belonging to each haplotype group). F, Purified proteins were subjected to SDS-PAGE and stained by Coomassie Brilliant Blue R-250. DCC1-WT from Col-0 was used as the control. DCC1-m175, DCC1-m481, and DCC1-m175/m481 were mutated according to Hap2 SNPs (SNP 175 and 481). G, Insulin reduction assay by the various proteins. Purified

We further performed linkage disequilibrium analyses using the nucleotide sequences of *DCC1* in 48 different ecotypes and found that six single-nucleotide polymorphisms (SNP 108, 147, 174, 175, 378, and 481) were highly associated with the shoot regeneration frequency (Fig. 11A). Two haplotypes (Hap1 and Hap2) of *DCC1* were identified among 48 natural variants of Arabidopsis. Hap1 included 30 ecotypes such as Col-0, Ws-0, Pu2-7, Lan-0, and Bu-0, and Hap2 included 18 ecotypes such as Gu-0, Nc-1, Keleterbach-4, Hn-0, and Su-0 (Fig. 11, A–C). The shoot regeneration frequencies and the number of shoots per callus were much higher in the Hap1 ecotypes than in the Hap2 ecotypes (Fig. 11, D and E), suggesting that this natural variation in *DCC1* is related to the regulation of shoot regeneration. Among the six SNPs, only two (SNP 175 and 481) resulted in the sense mutation (I59V and I161V) for the corresponding amino acids (Fig. 11, B and C). To identify the critical SNPs in *DCC1* among the natural variants, we detected the Trx activity by reduction of FiTC-insulin. Mutations at both positions 175 and 481 did not affect Trx activity of DCC1 (Fig. 11, F and G). Next, we performed yeast two-hybrid assays using *DCC1* with mutations at positions 175 and 481. We found that DCC1 did not interact with CA2 when there were mutations at both positions 175 and 481 (Fig. 11H). We also transformed a *pDCC1*:*DCC1-m175-m481* construct with *DCC1* mutated at positions 175 and 481 to rescue the *dcc1* mutant. The shoot regeneration frequencies in the *pDCC1*:*DCC1-m175-m481-dcc1* transgenic lines were not significantly different from those in *dcc1* (Fig. 11I), implying that SNP 175 and 481 of *DCC1* are critical for shoot regeneration.

Because DCC1 regulated shoot regeneration through ROS level, we assumed that DCC1-mediated ROS homeostasis might be involved in the natural variation in shoot regeneration among Arabidopsis ecotypes. To test this hypothesis, we detected the ROS levels in the Hap1 and Hap2 ecotypes by DAB staining (Fig. 12, A and B). The shoot regeneration frequencies and the number of shoots per callus were higher in the Hap1 ecotypes (Col-0, Kro-0, En-1, Ct-1, and Lp2-6) than in the Hap2 ecotypes (Bsch-0, Aa-0, Hn-0, Kelsterbach-4, and Gu-0; Fig. 12, C and D). Interestingly, the ROS levels were significantly lower in the Hap1 ecotypes than in the Hap2 ecotypes (Fig. 12E). These results suggest that DCC1-mediated ROS homeostasis is critical to the natural variation in shoot regeneration among Arabidopsis ecotypes.

DISCUSSION

Trxs belong to small proteins with a conserved CxxC motif throughout all organisms (Gelhaye et al., 2005; Meyer et al., 2005). Classic Trxs, such as Trx m, Trx o, Trx h, and Trx f, contain a motif of WCGPC or WCPPC, and atypical Trxs, such as APS REDUCTASE1 and HIGH CHLOROPHYLL FLUORESCENCE164, have a motif of WCPFC, HCGPC, or WCEVC (Gelhaye et al., 2005; Meyer et al., 2005). Trxs catalyze the reduction of the disulfide bond through these motifs and are critical to change the redox state of their target proteins (Rouhier et al., 2015). The redox state of ND3 (an important subunit of Complex I) determines the activity of Complex I (Galkin et al., 2008). Many subunits of mitochondrial respiratory Complex I (such as NAD7, NAD9, NDS8A, and NDUV2) are identified as potential targets of Trxs, but the direct evidence of redox regulation of these subunits by Trxs is missing (Balmer et al., 2004; Yoshida et al., 2013). In this study, we characterized a novel atypical Trx DCC1 that belongs to the DCC family of proteins. These proteins contain a conserved DxxCxxC motif (such as DGDCPLC, DGECPLC, or DGVCHLC) that differs from motifs of classic and atypical Trxs (Fig. 2B). DCC1 had the Trx activity determined by the reduction of insulin (Fig. 2D). CA2 is an essential subunit of Complex I (Soto et al., 2015) and was identified as a direct target of DCC1 (Fig. 5, A and B). DCC1 regulated Complex I activity by reduction of the CA2 complex (Fig. 5). Inhibition of Complex I activity caused by the mutation of *DCC1* or *CA2* triggered increased ROS production (Fig. 6), suggesting that DCC1 regulates Complex I activity and ROS homeostasis by redox regulation of CA2.

Many studies show that ROS can act as signaling factors regulating diverse processes (Rouhier et al., 2015; Schmidt and Schippers, 2015; Schippers et al., 2016). *NADPH-DEPENDENT THIOREDOXIN REDUCTASE A* (*NTRA*), *NADPH-DEPENDENT THIOREDOXIN REDUCTASE B* (*NTRB*), and the glutathione biosynthesis gene *CADMIUM SENSITIVE2* (*CAD2*) function to maintain ROS homeostasis, and the triple mutant *ntra ntrb cad2* generated an abnormal shoot meristem (Bashandy et al., 2010). Higher levels of ROS caused by the overexpression of *UP BEAT1* led to a short root meristem (Tsukagoshi et al., 2010). Elevated levels of ROS by the mutation of *KUODA1* led to a decreased leaf cell size (Lu et al., 2014). Here, we showed that increasing levels of ROS resulted in the inhibition of shoot regeneration (Figs. 6 and 7), whereas decreasing levels of ROS increased the capacity of shoot regeneration in the *dcc1*, *ca2*, and *dcc1ca2* mutants (Fig. 8). Thus,

Figure 11. (*Continued.*)
proteins were subjected to a reduction assay by using FiTC-insulin as the substrate, which displayed higher fluorescence after disulfide reduction. The assay mixture lacking recombinant proteins served as the control. Fluorescence intensity was recorded at 515- to 525-nm emission after 480- to 495-nm excitation for 120 min in a fluorescent plate reader at room temperature. H, Both SNP 175 and SNP 481 were critical for the interaction of DCC1 and CA2 by yeast two-hybrid assay. I, Frequencies of shoot regeneration from calli of wild-type Col-0, *dcc1*, *pDCC1*:*DCC1-dcc1*, and *pDCC1*:*DCC1-m175-m481-dcc1* on SIM at 28 d. Significant differences are indicated: **, $P < 0.01$ and ^{ns}, $P > 0.05$ (Student's one-tailed *t* test).

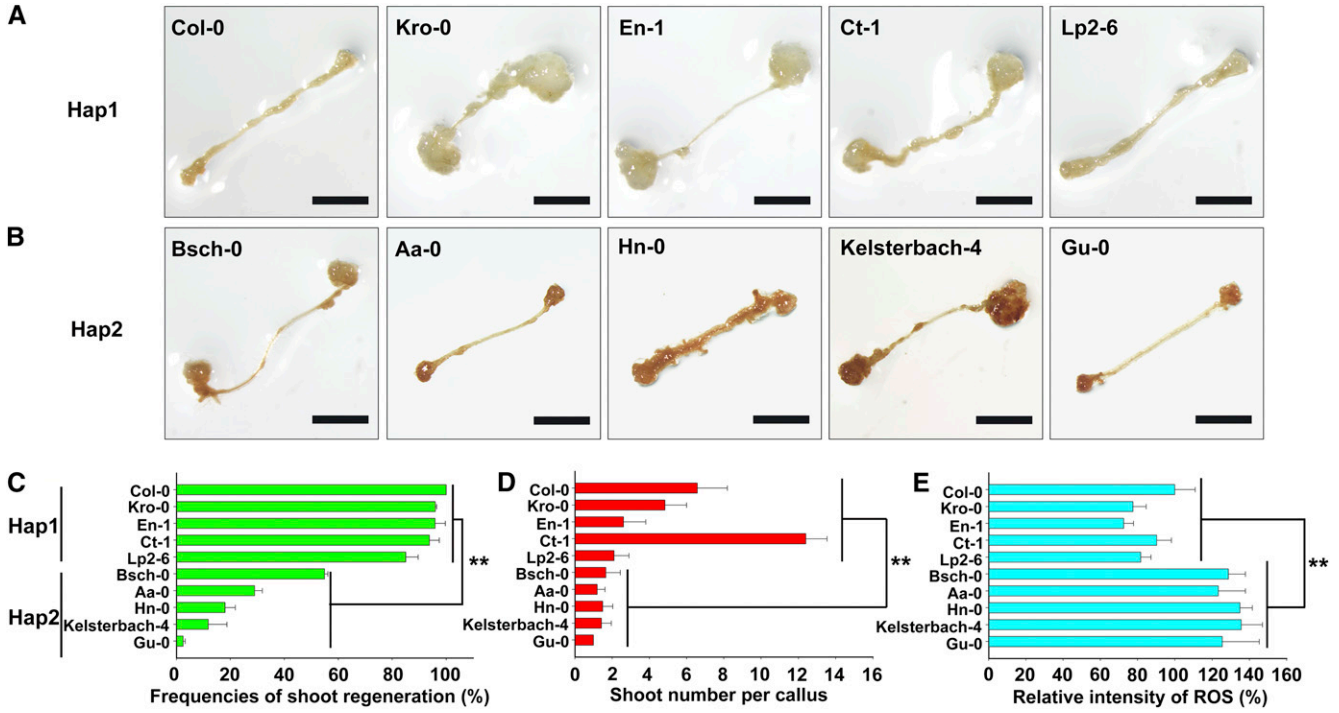

Figure 12. ROS levels are associated with the shoot regeneration capacities of different ecotypes in Arabidopsis. A, DAB staining showing ROS levels in calli of different ecotypes of Hap1 cultured on SIM at 16 d. B, DAB staining showing ROS levels in calli of different ecotypes of Hap2 cultured on SIM at 16 d. C, Shoot regeneration frequencies from calli of different ecotypes cultured on SIM at 28 d. D, Number of shoots per callus of different ecotypes cultured on SIM at 28 d. E, Relative staining intensity of ROS in calli of different ecotypes cultured on SIM at 16 d. SE values were calculated from three sets of biological replicates, and more than 100 calli were examined in each replicate. Asterisks indicate significant differences: **, $P < 0.01$ (Student's one-tailed *t* test). Bars = 500 μm.

ROS homeostasis is critical for the regulation of shoot regeneration.

Different mechanisms have been proposed to mediate the perception of ROS (Wrzaczek et al., 2013). An important mechanism is the one-component redox signaling system, which is based on redox-sensitive transcription factors (Schmidt and Schippers, 2015). Recent studies have identified a number of crucial redox-sensitive transcription factors, such as PHAVOLUTA for meristem development and organ polarity, BASIC REGION/LEUCINE ZIPPER TRANSCRIPTION FACTOR16 for light signaling, and TEOSINTE BRANCHED1-CYCLOIDEAPCF15 (TCP15) for auxin signaling (Schmidt and Schippers, 2015). Our results indicated that the increased ROS levels resulted in repressed expression of master genes for callus formation (*WOX5* and *WOX11*) and shoot meristem initiation (*WUS*, *CLV3*, and *STM*; Fig. 9). Moreover, auxin biosynthesis genes (*YUC4* and *TAA1*) were repressed by ROS (Fig. 10, C and D). Previously, it was shown that auxin was critical for shoot induction, and mutation of the auxin biosynthetic *YUC* genes repressed shoot regeneration (Gordon et al., 2007; Cheng et al., 2013). The redox-sensitive transcription factors TCPs regulate *YUC* expression and auxin biosynthesis (Viola et al., 2013; Lucero et al., 2015; Challa et al., 2016). Thus, it is likely that ROS regulates shoot regeneration by the redox modification of transcription factors involved in auxin biosynthesis and signaling.

The evolutionary adaptation of plants to environmental changes leads to diverse natural variation, which is critical for plant diversity (Mitchell-Olds and Schmitt, 2006). Natural variation causes a wide range of biological phenotypes and provides rich resources with which to analyze many important complex traits (Mitchell-Olds and Schmitt, 2006). A number of factors involved in natural variations have been identified in diverse biological processes, including regulation of flowering, seed development, and drought resistance (Johanson et al., 2000; Li et al., 2011b; Wang et al., 2016). FRIGIDA is a major determinant of the natural variation in Arabidopsis flowering time (Johanson et al., 2000). Natural variations in *GS5* can explain variations in rice (*Oryza sativa*) grain size and yield (Li et al., 2011b), and those in *ZmVPP1* contribute to the drought tolerance trait in maize (*Zea mays*; Wang et al., 2016). Here, we identified a major regulator, DCC1, that explains the variation in shoot regeneration capacity among natural variants of Arabidopsis (Fig. 11, A–E). The polymorphisms of *DCC1* were used to classify the different ecotypes of Arabidopsis into two groups: Hap1 and Hap2 (Fig. 11B). Interestingly, mutations at both critical SNPs (SNP 175 and 481) did not affect the Trx activity of DCC1 (Fig. 11G) but blocked the

interaction between DCC1 and CA2 (Fig. 11H), indicating that the two SNPs are critical for the function of DCC1, which is a major player in determining shoot regeneration capacity among natural variations.

MATERIALS AND METHODS

Plant Materials

The mutants *dcc1* (SALK_051222C) and *ca2* (SALK_010194C), line MT-GK (CS16263), and different ecotypes of Arabidopsis (*Arabidopsis thaliana*) were obtained from the Arabidopsis Biological Resource Center. *DR5rev*:*GFP* lines were generously provided by Dr. Jian Xu (Department of Biological Science, National University of Singapore; Xu et al., 2006).

Shoot Regeneration

The shoot regeneration experiment was performed as described previously (Li et al., 2011a). Seeds were placed on germination medium after sterilization in 70% (v/v) ethanol for 5 min and 2.6% (v/v) sodium hypochlorite for 10 min. All the seeds were stratified at 4°C for 3 d and then grown for 12 d in a growth chamber at 22°C under a 16-h-light/8-h-dark photoperiod. Root segments (5–10 mm) were cut and placed on CIM (Gamborg's B5 medium supplemented with 0.5 g L^{-1} MES, 2% [w/v] Glc, 0.2 μM kinetin, 2.2 μM 2,4-dichlorophenoxyacetic acid, and 0.8% [w/v] agar). After the explants were incubated in continuous light for 6 d, the calli were transferred onto SIM (Gamborg's B5 medium supplemented with 0.5 g L^{-1} MES, 2% [w/v] Glc, 0.9 μM 3-indoleacetic acid, 0.5 μM 2-isopentenyladenine, and 0.8% [w/v] agar) and incubated in continuous light. The calli were transferred onto fresh medium every 6 d. Images of calli were acquired using an Olympus DP72 microscope. The shoots on each callus were defined as being at least 2 mm long. Shoot regeneration frequency (%) was calculated as follows: number of calli with at least one shoot/total number of calli cultured on SIM × 100. Three sets of biological replicates were used in the calculations, and more than 100 calli were examined in each replicate.

Plasmid Construction

The oligonucleotide primers for all constructs are given in Supplemental Table S4. For phenotypic complementation and GUS signal analyses, *DCC1* or *CA2* genomic fragments including the promoter and gene were introduced into *pMDC99* to construct *ProDCC1*:*DCC1* and *ProCA2*:*CA2*, respectively, and into *pMDC163* to obtain *ProDCC1*:*DCC1-GUS* and *ProCA2*:*CA2-GUS*, respectively. For subcellular localization, *DCC1* cDNA was cloned into *pH7RWG2* to generate *35S*:*DCC1-RFP* by Gateway technology (Karimi et al., 2002). For the yeast two-hybrid constructs, cDNAs of *DCC1* and *CA2* without the signal peptide sequence were cloned into *pGADT7* and *pGBKT7* to generate *DCC1-AD* and *CA2-BD*, respectively. For the pull-down assay, cDNAs of *DCC1* and *CA2* without the signal peptide sequence were cloned into *pET28a* and *pGEX-4T-1* to generate *DCC1-His* and *CA2-GST*, respectively. For the firefly luciferase complementation assay, gene sequences of *DCC1* and *CA2* were cloned into *p1300-nLUC* and *p1300-cLUC* to generate *35S*:*DCC1-nLUC* and *35S*:*CA2-cLUC*, respectively. For the coimmunoprecipitation, gene sequences of *DCC1* and *CA2* were introduced into *pEarlyGate103* and *pEarlyGate203* to generate *35S*:*DCC1-GFP* and *35S*:*CA2-MYC*, respectively. For the reduction of CA2, cDNA of DCC1 without the signal peptide sequence was cloned into *pGEX-4T-1* to generate *DCC1-GST*. For *CAT3* overexpression, *CAT3* cDNA was amplified and cloned into *pER8* to construct *pER8-CAT3*.

For the construct *pDCC1*:*DCC1-m175-m481*, the *DCC1* promoter sequence was amplified using the primer DCC1-F7/R7 and cloned into *pBI121*. *DCC1-m175-m481* (m175 indicates mutation at position 175 of the *DCC1* gene) fragments were amplified using primers (DCC1-F8/R8, DCC1-F9/R9, and DCC1-F10/R10) by overlap-extension two-step PCR mutagenesis and introduced into *pBI121* containing the *DCC1* promoter. For DCC1 Trx activity determination, DCC1-m175-His (with primer DCC1-F11/R11), DCC1-m481-His (with primers DCC1-F12/R12 and DCC1-F13/R13), and DCC1-m175-m481-His (with primers DCC1-F11/R12 and DCC1-F13/R13) were generated by overlap-extension two-step PCR mutagenesis and inserted into *pET28a* for protein purification. For yeast hybrid interaction, DCC1-m175-AD (with primer DCC1-F14/R14), DCC1-m481-AD (with primers DCC1-F15/R15 and DCC1-F16/R16), and DCC1-m175-m481-AD (with primers DCC1-F14/R15 and DCC1-F16/R16) were amplified by overlap-extension two-step PCR mutagenesis and inserted into pGADT7 for yeast hybrid interaction.

GUS Staining Assay

We conducted GUS staining assays as described elsewhere (Sieburth and Meyerowitz, 1997; Su et al., 2009). Briefly, calli were incubated in GUS assay buffer at 37°C for 10 h and then fixed in 70% (v/v) ethanol at room temperature. The calli were embedded in paraffin and cut into 10-μm sections. Ruthenium Red (0.2 g L^{-1}) was used to stain cell walls.

Confocal Microscopy

MT-GK is a reported marker line specially expressing Mito-GFP (Nelson et al., 2007). To determine the subcellular localization of DCC1, the construct *35S*:*DCC1-RFP* was introduced into MT-GK. The roots of the T1 transgenetic lines were excised for imaging by a Leica TCS SP5 confocal microscope. The DCC1-RFP signal was observed at 505- to 550-nm emission after 561-nm excitation, whereas the Mito-GFP signal was observed at 570- to 620-nm emission after 488-nm excitation. The merged signals of GFP and RFP showed yellow color. To detect the auxin response pattern, approximately 60 calli cultured on SIM at different times were sampled to observe the expression of *DR5rev*:*GFP*. The calli were cut into 1- to 2-mm sections along the longitudinal axis, and the sections were viewed with a Leica TCS SP5 confocal microscope. The GFP signal was observed at 505- to 550-nm emission after 488-nm excitation.

Phylogenetic Analysis

Phylogenetic analysis used DCC1 (NP_568719.1) with its homologs in *Camelina sativa* (XP_010441588.1), *Brassica rapa* (XP_010441588.1), *Raphanus sativus* (XP_018455194.1), *Gossypium hirsutum* (XP_016755751.1), *Ziziphus jujuba* (XP_015882648.1), *Malus domestica* (XP_008393058.1), *Prunus persica* (XP_007209569.1), *Oryza officinalis* (XP_015633461.1), *Zea mays* (XP_008663715.1), *Physcomitrella patens* (XP_001777984.1), *Populus trichocarpa* (XP_002322151.2), *Vitis vinifera* (XP_002283569.1), *Triticum urartu* (EMS60538.1), *Microcystis aeruginosa* (WP_002792509.1), Arabidopsis (AT1G52590 [NP_564611.1] and AT1G24095 [NP_001185076.1]), *Caulobacter crescentus* (NP_422377.1), *Bacillus halodurans* (WP_010897025.1), and *Pseudomonas aeruginosa* (NP_249825.1). The analysis was performed by MEGA 5.1 software. The protein sequences were downloaded from the National Center for Biotechnology Information database.

Trx Activity Assay

The construct *pET28a-DCC1* was transferred into Rosetta competent cells. DCC1-His proteins were induced by incubation in 1 mM IPTG at 22°C with shaking at 120 rpm for 16 h. The cell pellet was resuspended in buffer (25 mM Tris, pH 7.5, and 0.5 mM DTT; Motohashi et al., 2003). Protein purification was performed using Ni Sepharose 6 Fast Flow (GE Healthcare; catalog no. 28-9355-97). Then, the proteins were dialyzed against buffer (25 mM Tris, pH 7.5) to remove imidazole using Slide-A-Lyzer Dialysis Cassettes (Thermo Fisher Scientific; catalog no. 66810) for 24 h. Trx activity was measured using the Thioredoxin Activity Fluorescent Assay Kit (Cayman Chemicals; catalog no. 11527). The FiTC-insulin in the kit was used as the substrate of DCC1. FiTC displays higher fluorescence after disulfide reduction (Montano et al., 2014). The reduction assay was performed by incubation with purified DCC1 protein (10 μg). NADPH and TrxR were used to recycle the DCC1 Trx activity. The reaction mixture without DCC1 proteins was used as the control. The fluorescence intensity of each sample was recorded at 515- to 525-nm emission after excitation at 480 to 495 nm for 60 min using the BioTek Synergy 2 Multi-Mode Reader (BioTek) at ambient room temperature. Three sets of biological replicates were performed for each reaction.

Yeast Two-Hybrid Assay

The yeast two-hybrid assay was performed using the Matchmaker Gold Yeast Two-Hybrid System (Clontech; catalog no. 630489) according to the manufacturer's instructions. The constructs *DCC1-AD* and *CA2-BD* were cotransferred into Y2H Gold competent cells. Activation was observed at 3 d on selection plates (SD/-Leu-Trp-His-Ade) with X-α-gal.

Firefly Luciferase Complementation Assay

Firefly luciferase complementation assays were conducted as described previously (Li et al., 2014). The constructs *DCC1-nLUC* and *CA2-cLUC* were transformed into leaves of *Nicotiana benthamiana* for transient expression. Transfected leaves were sprayed with buffer (1 mM D-luciferin sodium salt and 0.1% [v/v] Triton X-100) 5 min before being imaged using the IVIS Lumina II system (Caliper Life Sciences).

Pull-Down Assay

For the pull-down assay, 10 μg of CA2-GST protein was incubated with 10 μL of glutathione-Sepharose-4B beads (GE Healthcare; catalog no. 17-0756-01) in blocking buffer (140 mM NaCl, 2.7 mM KCl, 10 mM Na_2HPO_4, 1.8 mM KH_2PO_4, 0.1% [w/v] Nonidet P-40, and 1 g of BSA) under agitation at 4°C for 2 h. Then, 1 μg of DCC1-His protein was added, and the mixture was incubated for 2 h in binding buffer (140 mM NaCl, 2.7 mM KCl, 10 mM Na_2HPO_4, 1.8 mM KH_2PO_4, and 0.1% [w/v] Nonidet P-40). The beads were washed 10 times with washing buffer (400 mM NaCl, 2.7 mM KCl, 10 mM Na_2HPO_4, 1.8 mM KH_2PO_4, and 0.1% [v/v] Nonidet P-40). Finally, 10% input and pull-down proteins were separated by 12% SDS-PAGE and detected by immunoblotting using the antibodies anti-His, diluted 1:3,000 (Sigma; catalog no. H1029), or anti-GST, diluted 1:3,000 (Sigma; catalog no. G1160).

Coimmunoprecipitation Assay

We used transgenic seedlings of *35S:DCC1-GFP* and the F1 generation of *35S:DCC1-GFP* × *35S:CA2-MYC* for immunoprecipitation analyses. Proteins were extracted from 2 g of seedlings with extraction buffer (140 mM NaCl, 2.7 mM KCl, 10 mM Na_2HPO_4, 1.8 mM KH_2PO_4, 0.1 mM EDTA, 0.1% [v/v] Nonidet P-40, 5 mM DTT, and 0.5 mM PMSF). Then, 60 μL of beads was incubated with 10 μL of anti-GFP antibody with agitation for 2 h at 4°C. Then, supernatants were added and incubated with agitation for 8 h at 4°C. After incubation, beads were washed 10 times with washing buffer (400 mM NaCl, 2.7 mM KCl, 10 mM Na_2HPO_4, 1.8 mM KH_2PO_4, 0.1 mM EDTA, 0.1% [v/v] Nonidet P-40, 5 mM DTT, and 0.5 mM phenylmethylsulfonyl fluoride). Finally, 10% input and immunoprecipitation proteins were separated by 12% SDS-PAGE and detected by immunoblotting using the antibodies anti-MYC, diluted 1:1,000 (Sigma; catalog no. M4439), or anti-GFP, diluted 1:1,000 (Roche; catalog no. 11814460001).

Reduction of CA2 by DCC1

The reduction assay was performed as described previously with slight modifications (Yoshida et al., 2015). The GST tag of the recombinant DCC1-GST proteins was cleaved by a thrombin (Sigma; catalog no. T9326). Purified CA2-His protein (1 μM) was incubated with GST-cleaved DCC1 protein in the assay mixture containing 50 mM Tris-HCl (pH 7.5) and 50 mM NaCl. DTT (0.3 mM) was added to recycle DCC1 Trx activity. The mixture without DCC1 proteins was used as the control. After incubation for 30 min at 25°C, proteins were subjected to nonreducing (without 2-mercaptoethanol) or reducing (with 2-mercaptoethanol) SDS-PAGE followed by immunoblot analysis using anti-His antibody diluted 1:5,000 (Sigma; catalog no. H1029).

Mitochondrial Respiratory Complex I Activity Assay

Calli (0.1 g) of wild-type Col-0, *dcc1*, *ca2*, and *dcc1ca2* cultured on SIM at 16 d were collected, and then the mitochondria were isolated using the Plant Mitochondria Isolation Kit (Biohao; catalog no. P0045) according to the manufacturer's instructions. Mitochondrial respiratory Complex I activity was determined using 20 μg of mitochondrial protein with the MitoCheck Complex I Activity Assay Kit (Cayman Chemicals; catalog no. 700930). The absorbance of all samples was measured at 340 nm for 60 min using a plate reader. Complex I activity was calculated from the decrease in absorbance per minute. SE values were calculated from three sets of biological replicates.

Chemical Treatments

Chemical reagents were added to the medium before transfer of calli, and calli were transferred to new medium with fresh reagents every 6 d. Different concentrations of H_2O_2 (0.005‰ and 0.01‰) or GSH (100, 300, and 600 μM) were added to the shoot regeneration system, and 10 μM estradiol was added to induce the transcription of *CAT3* to complement the phenotypes of *dcc1*, *ca2*, and *dcc1ca2*.

DAB Staining Assay

Calli were incubated in DAB staining buffer (50 mM Tris, pH 7.6, and 0.6 mg mL^{-1} DAB) at room temperature in darkness and then fixed in 70% (v/v) ethanol at room temperature. The calli were observed with an Olympus DP72 microscope until the chlorophyll disappeared. The relative DAB staining intensity was analyzed by ImageJ software. Three sets of biological replicates were calculated, and more than 30 calli were examined in each replicate.

Quantitative Real-Time PCR

Total RNA was isolated using TRI reagent (Sigma; catalog no. T9424) and treated with DNase I (Thermo Fisher Scientific; catalog no. EN0521). Then, cDNAs were synthesized using M-MLV reverse transcriptase (Promega; catalog no. M1701). The qRT-PCR assays were conducted using the CFX96 Real-Time PCR Detection System (Bio-Rad) in a 20-μL reaction volume with 45 cycles. The cDNA levels were normalized against those of two housekeeping genes, *TUB2* and *ACTIN2*. The relative expression level of each gene was standardized to *TUB2* and calculated using the comparative C_T method (Schmittgen and Livak, 2008). Mean values were calculated from three biological replicates. The sequences of primers used for qRT-PCR are listed in Supplemental Table S4.

RNA Sequencing and Data Analyses

Three biological repeats of the wild type (Col-0-A, Col-0-B, and Col-0-C) and the *dcc1* mutant (*dcc1*-A, *dcc1*-B, and *dcc1*-C) were used for RNA sequencing. Total RNAs were isolated from the calli of wild-type Col-0 and *dcc1* cultured on SIM at 16 d with TRI reagent (Sigma; catalog no. T9424). RNA was sequenced using the Illumina 2500 instrument in Gene Denovo Biotechnology. The raw reads were aligned to the genome sequences of TAIR10 (www.arabidopsis.org) using Tophat2 software (version 2.0.3.12; Kim et al., 2013). The gene expression levels were measured in FPKM using Cufflinks software (Trapnell et al., 2012). Statistical analyses were performed using the edgeR package (https://www.r-project.org/). Differentially expressed genes were those with fold change ≥ 2 and FDR < 0.05 between the wild-type Col-0 and the mutant *dcc1*. A GO enrichment analysis was performed in the GO database (http://www.geneontology.org/; Ashburner et al., 2000). The RNA sequencing data are available in the ArrayExpress database (www.ebi.ac.uk/arrayexpress) under the accession number E-MTAB-5236.

Linkage Disequilibrium Analyses

Linkage disequilibrium analyses were performed using Genome Variation Server (Carlson et al., 2004) with *DCC1* nucleotide sequences from 48 ecotypes of Arabidopsis.

Accession Numbers

Sequence data from this article can be found in the GenBank/EMBL data libraries under accession numbers AT5G50100 (DCC1), AT1G47260 (CA2), AT3G11260 (WOX5), AT3G03660 (WOX11), AT5G17810 (WOX12), AT5G10510 (PLT3), AT5G57390 (PLT5), AT2G42430 (LBD16), AT2G42440 (LBD17), AT2G45420 (LBD18), AT3G58190 (LBD29), AT1G78080 (WIND1), AT2G17950 (WUS), AT2G27250 (CLV3), and AT1G62360 (STM).

Supplemental Data

The following supplemental materials are available.

Supplemental Figure S1. Identification of the *dcc1* mutant.

Supplemental Figure S2. Phenotypes of the double mutant *dcc1ca2* during shoot regeneration.

Supplemental Figure S3. Exogenous GSH promotes shoot regeneration.

Supplemental Figure S4. Transcript level of *CAT3* in *CAT3*-overexpressing transgenic lines.

Supplemental Figure S5. Correlations among three biological repeats of RNA-seq analyses.

Supplemental Figure S6. Analyses of differentially expressed genes identified by RNA-seq were confirmed by qRT-PCR.

Supplemental Figure S7. Shoot regeneration capacity of different Arabidopsis ecotypes.

Supplemental Table S1. Frequencies of shoot regeneration in the Trx mutants.

Supplemental Table S2. Up-regulated genes in the *dcc1* mutant as determined by RNA-seq analyses.

Supplemental Table S3. Down-regulated genes in the *dcc1* mutant as determined by RNA-seq analyses.

Supplemental Table S4. Sequences of primers used in this study.

ACKNOWLEDGMENTS

We thank all who generously provided plant materials in this research. We thank Dr. Min Ni (Department of Plant Biology, University of Minnesota) for critical reading of the article.

Received June 19, 2017; accepted July 17, 2017; published January 29, 2018.

LITERATURE CITED

Arabidopsis Interactome Mapping Consortium (2011) Evidence for network evolution in an *Arabidopsis* interactome map. Science **333:** 601–607

Ashburner M, Ball CA, Blake JA, Botstein D, Butler H, Cherry JM, Davis AP, Dolinski K, Dwight SS, Eppig JT, et al (2000) Gene Ontology: tool for the unification of biology. Nat Genet **25:** 25–29

Balmer Y, Vensel WH, Tanaka CK, Hurkman WJ, Gelhaye E, Rouhier N, Jacquot JP, Manieri W, Schürmann P, Droux M, et al (2004) Thioredoxin links redox to the regulation of fundamental processes of plant mitochondria. Proc Natl Acad Sci USA **101:** 2642–2647

Bashandy T, Guilleminot J, Vernoux T, Caparros-Ruiz D, Ljung K, Meyer Y, Reichheld JP (2010) Interplay between the NADP-linked thioredoxin and glutathione systems in *Arabidopsis* auxin signaling. Plant Cell **22:** 376–391

Benitez-Alfonso Y, Cilia M, San Roman A, Thomas C, Maule A, Hearn S, Jackson D (2009) Control of Arabidopsis meristem development by thioredoxin-dependent regulation of intercellular transport. Proc Natl Acad Sci USA **106:** 3615–3620

Birnbaum KD, Alvarado AS (2008) Slicing across kingdoms: regeneration in plants and animals. Cell **132:** 697–710

Braun HP, Binder S, Brennicke A, Eubel H, Fernie AR, Finkemeier I, Klodmann J, König AC, Kühn K, Meyer E, et al (2014) The life of plant mitochondrial complex I. Mitochondrion **19:** 295–313

Carlson CS, Eberle MA, Rieder MJ, Yi Q, Kruglyak L, Nickerson DA (2004) Selecting a maximally informative set of single-nucleotide polymorphisms for association analyses using linkage disequilibrium. Am J Hum Genet **74:** 106–120

Challa KR, Aggarwal P, Nath U (2016) Activation of *YUCCA5* by the transcription factor TCP4 integrates developmental and environmental signals to promote hypocotyl elongation in *Arabidopsis*. Plant Cell **2016:** 2016

Cheng ZJ, Wang L, Sun W, Zhang Y, Zhou C, Su YH, Li W, Sun TT, Zhao XY, Li XG, et al (2013) Pattern of auxin and cytokinin responses for shoot meristem induction results from the regulation of cytokinin biosynthesis by AUXIN RESPONSE FACTOR3. Plant Physiol **161:** 240–251

Considine MJ, Foyer CH (2014) Redox regulation of plant development. Antioxid Redox Signal **21:** 1305–1326

Dietz KJ, Turkan I, Krieger-Liszkay A (2016) Redox- and reactive oxygen species-dependent signaling into and out of the photosynthesizing chloroplast. Plant Physiol **171:** 1541–1550

Dos Santos CV, Rey P (2006) Plant thioredoxins are key actors in the oxidative stress response. Trends Plant Sci **11:** 329–334

Dröse S, Brandt U, Wittig I (2014) Mitochondrial respiratory chain complexes as sources and targets of thiol-based redox-regulation. Biochim Biophys Acta **1844:** 1344–1354

Duclercq J, Sangwan-Norreel B, Catterou M, Sangwan RS (2011) *De novo* shoot organogenesis: from art to science. Trends Plant Sci **16:** 597–606

Fan M, Xu C, Xu K, Hu Y (2012) LATERAL ORGAN BOUNDARIES DOMAIN transcription factors direct callus formation in *Arabidopsis* regeneration. Cell Res **22:** 1169–1180

Galkin A, Meyer B, Wittig I, Karas M, Schägger H, Vinogradov A, Brandt U (2008) Identification of the mitochondrial ND3 subunit as a structural component involved in the active/deactive enzyme transition of respiratory complex I. J Biol Chem **283:** 20907–20913

Gelhaye E, Rouhier N, Navrot N, Jacquot JP (2005) The plant thioredoxin system. Cell Mol Life Sci **62:** 24–35

Ginalski K, Kinch L, Rychlewski L, Grishin NV (2004) DCC proteins: a novel family of thiol-disulfide oxidoreductases. Trends Biochem Sci **29:** 339–342

Gordon SP, Heisler MG, Reddy GV, Ohno C, Das P, Meyerowitz EM (2007) Pattern formation during *de novo* assembly of the *Arabidopsis* shoot meristem. Development **134:** 3539–3548

Hagen G, Guilfoyle T (2002) Auxin-responsive gene expression: genes, promoters and regulatory factors. Plant Mol Biol **49:** 373–385

Huang S, Van Aken O, Schwarzländer M, Belt K, Millar AH (2016) The roles of mitochondrial reactive oxygen species in cellular signaling and stress response in plants. Plant Physiol **171:** 1551–1559

Ikeuchi M, Ogawa Y, Iwase A, Sugimoto K (2016) Plant regeneration: cellular origins and molecular mechanisms. Development **143:** 1442–1451

Iwase A, Mitsuda N, Koyama T, Hiratsu K, Kojima M, Arai T, Inoue Y, Seki M, Sakakibara H, Sugimoto K, et al (2011) The AP2/ERF transcription factor WIND1 controls cell dedifferentiation in *Arabidopsis*. Curr Biol **21:** 508–514

Johanson U, West J, Lister C, Michaels S, Amasino R, Dean C (2000) Molecular analysis of *FRIGIDA*, a major determinant of natural variation in *Arabidopsis* flowering time. Science **290:** 344–347

Kareem A, Durgaprasad K, Sugimoto K, Du Y, Pulianmackal AJ, Trivedi ZB, Abhayadev PV, Pinon V, Meyerowitz EM, Scheres B, et al (2015) *PLETHORA* genes control regeneration by a two-step mechanism. Curr Biol **25:** 1017–1030

Karimi M, Inzé D, Depicker A (2002) GATEWAY vectors for Agrobacterium-mediated plant transformation. Trends Plant Sci **7:** 193–195

Kim D, Pertea G, Trapnell C, Pimentel H, Kelley R, Salzberg SL (2013) TopHat2: accurate alignment of transcriptomes in the presence of insertions, deletions and gene fusions. Genome Biol **14:** R36

Kimura S, Waszczak C, Hunter K, Wrzaczek M (2017) Bound by fate: the role of reactive oxygen species in receptor-like kinase signaling. Plant Cell **29:** 638–654

Lall S, Nettleton D, DeCook R, Che P, Howell SH (2004) Quantitative trait loci associated with adventitious shoot formation in tissue culture and the program of shoot development in *Arabidopsis*. Genetics **167:** 1883–1892

Li W, Liu H, Cheng ZJ, Su YH, Han HN, Zhang Y, Zhang XS (2011a) DNA methylation and histone modifications regulate *de novo* shoot regeneration in *Arabidopsis* by modulating *WUSCHEL* expression and auxin signaling. PLoS Genet **7:** e1002243

Li XR, Li HJ, Yuan L, Liu M, Shi DQ, Liu J, Yang WC (2014) *Arabidopsis* DAYU/ABERRANT PEROXISOME MORPHOLOGY9 is a key regulator of peroxisome biogenesis and plays critical roles during pollen maturation and germination in planta. Plant Cell **26:** 619–635

Li Y, Fan C, Xing Y, Jiang Y, Luo L, Sun L, Shao D, Xu C, Li X, Xiao J, et al (2011b) Natural variation in GS5 plays an important role in regulating grain size and yield in rice. Nat Genet **43:** 1266–1269

Liu J, Sheng L, Xu Y, Li J, Yang Z, Huang H, Xu L (2014) WOX11 and 12 are involved in the first-step cell fate transition during *de novo* root organogenesis in *Arabidopsis*. Plant Cell **26:** 1081–1093

Lu D, Wang T, Persson S, Mueller-Roeber B, Schippers JH (2014) Transcriptional control of ROS homeostasis by KUODA1 regulates cell expansion during leaf development. Nat Commun **5:** 3767

Lu J, Holmgren A (2014) The thioredoxin antioxidant system. Free Radic Biol Med **66:** 75–87

Lucero LE, Uberti-Manassero NG, Arce AL, Colombatti F, Alemano SG, Gonzalez DH (2015) TCP15 modulates cytokinin and auxin responses during gynoecium development in *Arabidopsis*. Plant J **84:** 267–282

Mangano S, Juárez SPD, Estevez JM (2016) ROS regulation of polar growth in plant cells. Plant Physiol **171:** 1593–1605

Meng L, Wong JH, Feldman LJ, Lemaux PG, Buchanan BB (2010) A membrane-associated thioredoxin required for plant growth moves

from cell to cell, suggestive of a role in intercellular communication. Proc Natl Acad Sci USA **107:** 3900–3905

Meng WJ, Cheng ZJ, Sang YL, Zhang MM, Rong XF, Wang ZW, Tang YY, Zhang XS (2017) Type-B ARABIDOPSIS RESPONSE REGULATORs specify the shoot stem cell niche by dual regulation of WUSCHEL. Plant Cell **29:** 1357–1372

Meyer Y, Reichheld JP, Vignols F (2005) Thioredoxins in *Arabidopsis* and other plants. Photosynth Res **86:** 419–433

Mitchell-Olds T, Schmitt J (2006) Genetic mechanisms and evolutionary significance of natural variation in *Arabidopsis*. Nature **441:** 947–952

Montano SJ, Lu J, Gustafsson TN, Holmgren A (2014) Activity assays of mammalian thioredoxin and thioredoxin reductase: fluorescent disulfide substrates, mechanisms, and use with tissue samples. Anal Biochem **449:** 139–146

Montrichard F, Alkhalfioui F, Yano H, Vensel WH, Hurkman WJ, Buchanan BB (2009) Thioredoxin targets in plants: the first 30 years. J Proteomics **72:** 452–474

Motohashi K, Koyama F, Nakanishi Y, Ueoka-Nakanishi H, Hisabori T (2003) Chloroplast cyclophilin is a target protein of thioredoxin: thiol modulation of the peptidyl-prolyl cis-trans isomerase activity. J Biol Chem **278:** 31848–31852

Motte H, Vercauteren A, Depuydt S, Landschoot S, Geelen D, Werbrouck S, Goormachtig S, Vuylsteke M, Vereecke D (2014) Combining linkage and association mapping identifies *RECEPTOR-LIKE PROTEIN KINASE1* as an essential *Arabidopsis* shoot regeneration gene. Proc Natl Acad Sci USA **111:** 8305–8310

Murmu J, Bush MJ, DeLong C, Li S, Xu M, Khan M, Malcolmson C, Fobert PR, Zachgo S, Hepworth SR (2010) Arabidopsis basic leucine-zipper transcription factors TGA9 and TGA10 interact with floral glutaredoxins ROXY1 and ROXY2 and are redundantly required for anther development. Plant Physiol **154:** 1492–1504

Nelson BK, Cai X, Nebenführ A (2007) A multicolored set of *in vivo* organelle markers for co-localization studies in *Arabidopsis* and other plants. Plant J **51:** 1126–1136

Rogers H, Munné-Bosch S (2016) Production and scavenging of reactive oxygen species and redox signaling during leaf and flower senescence: similar but different. Plant Physiol **171:** 1560–1568

Rouhier N, Cerveau D, Couturier J, Reichheld JP, Rey P (2015) Involvement of thiol-based mechanisms in plant development. Biochim Biophys Acta **1850:** 1479–1496

Sandalio LM, Romero-Puertas MC (2015) Peroxisomes sense and respond to environmental cues by regulating ROS and RNS signalling networks. Ann Bot **116:** 475–485

Schiantarelli E, De la Peña A, Candela M (2001) Use of recombinant inbred lines (RILs) to identify, locate and map major genes and quantitative trait loci involved with *in vitro* regeneration ability in *Arabidopsis thaliana*. Theor Appl Genet **102:** 335–341

Schippers JH, Foyer CH, van Dongen JT (2016) Redox regulation in shoot growth, SAM maintenance and flowering. Curr Opin Plant Biol **29:** 121–128

Schmidt R, Schippers JH (2015) ROS-mediated redox signaling during cell differentiation in plants. Biochim Biophys Acta **1850:** 1497–1508

Schmittgen TD, Livak KJ (2008) Analyzing real-time PCR data by the comparative C(T) method. Nat Protoc **3:** 1101–1108

Scofield S, Dewitte W, Murray JAH (2007) The *KNOX* gene *SHOOT MERISTEMLESS* is required for the development of reproductive meristematic tissues in *Arabidopsis*. Plant J **50:** 767–781

Sieburth LE, Meyerowitz EM (1997) Molecular dissection of the AGAMOUS control region shows that cis elements for spatial regulation are located intragenically. Plant Cell **9:** 355–365

Soto D, Córdoba JP, Villarreal F, Bartoli C, Schmitz J, Maurino VG, Braun HP, Pagnussat GC, Zabaleta E (2015) Functional characterization of mutants affected in the carbonic anhydrase domain of the respiratory complex I in *Arabidopsis thaliana*. Plant J **83:** 831–844

Staswick PE, Serban B, Rowe M, Tiryaki I, Maldonado MT, Maldonado MC, Suza W (2005) Characterization of an *Arabidopsis* enzyme family that conjugates amino acids to indole-3-acetic acid. Plant Cell **17:** 616–627

Su YH, Zhao XY, Liu YB, Zhang CL, O'Neill SD, Zhang XS (2009) Auxin-induced *WUS* expression is essential for embryonic stem cell renewal during somatic embryogenesis in *Arabidopsis*. Plant J **59:** 448–460

Sugimoto K, Jiao Y, Meyerowitz EM (2010) *Arabidopsis* regeneration from multiple tissues occurs via a root development pathway. Dev Cell **18:** 463–471

Tada Y, Spoel SH, Pajerowska-Mukhtar K, Mou Z, Song J, Wang C, Zuo J, Dong X (2008) Plant immunity requires conformational changes [corrected] of NPR1 via S-nitrosylation and thioredoxins. Science **321:** 952–956

Trapnell C, Roberts A, Goff L, Pertea G, Kim D, Kelley DR, Pimentel H, Salzberg SL, Rinn JL, Pachter L (2012) Differential gene and transcript expression analysis of RNA-seq experiments with TopHat and Cufflinks. Nat Protoc **7:** 562–578

Tsukagoshi H, Busch W, Benfey PN (2010) Transcriptional regulation of ROS controls transition from proliferation to differentiation in the root. Cell **143:** 606–616

van der Graaff E, Laux T, Rensing SA (2009) The WUS homeobox-containing (WOX) protein family. Genome Biol **10:** 248

Velázquez I, Valencia S, López-Lera A, de la Peña A, Candela M (2004) Analysis of natural allelic variation in *in vitro* organogenesis of *Arabidopsis thaliana*. Euphytica **137:** 73–79

Viola IL, Güttlein LN, Gonzalez DH (2013) Redox modulation of plant developmental regulators from the class I TCP transcription factor family. Plant Physiol **162:** 1434–1447

Wang X, Wang H, Liu S, Ferjani A, Li J, Yan J, Yang X, Qin F (2016) Genetic variation in *ZmVPP1* contributes to drought tolerance in maize seedlings. Nat Genet **48:** 1233–1241

Waszczak C, Akter S, Jacques S, Huang J, Messens J, Van Breusegem F (2015) Oxidative post-translational modifications of cysteine residues in plant signal transduction. J Exp Bot **66:** 2923–2934

Wrzaczek M, Brosché M, Kangasjärvi J (2013) ROS signaling loops: production, perception, regulation. Curr Opin Plant Biol **16:** 575–582

Xie HT, Wan ZY, Li S, Zhang Y (2014) Spatiotemporal production of reactive oxygen species by NADPH oxidase is critical for tapetal programmed cell death and pollen development in *Arabidopsis*. Plant Cell **26:** 2007–2023

Xu J, Hofhuis H, Heidstra R, Sauer M, Friml J, Scheres B (2006) A molecular framework for plant regeneration. Science **311:** 385–388

Yoshida K, Hara S, Hisabori T (2015) Thioredoxin selectivity for thiol-based redox regulation of target proteins in chloroplasts. J Biol Chem **290:** 14278–14288

Yoshida K, Noguchi K, Motohashi K, Hisabori T (2013) Systematic exploration of thioredoxin target proteins in plant mitochondria. Plant Cell Physiol **54:** 875–892

Yu Q, Tian H, Yue K, Liu J, Zhang B, Li X, Ding Z (2016) A P-loop NTPase regulates quiescent center cell division and distal stem cell identity through the regulation of ROS homeostasis in *Arabidopsis* root. PLoS Genet **12:** e1006175

Zhang TQ, Lian H, Zhou CM, Xu L, Jiao Y, Wang JW (2017) A two-step model for de novo activation of WUSCHEL during plant shoot regeneration. Plant Cell **29:** 1073–1087

Zhao Y (2010) Auxin biosynthesis and its role in plant development. Annu Rev Plant Biol **61:** 49–64

Zou JJ, Li XD, Ratnasekera D, Wang C, Liu WX, Song LF, Zhang WZ, Wu WH (2015) *Arabidopsis* CALCIUM-DEPENDENT PROTEIN KINASE8 and CATALASE3 function in abscisic acid-mediated signaling and H_2O_2 homeostasis in stomatal guard cells under drought stress. Plant Cell **27:** 1445–1460